

THESIS

AUTOMATED SAMPLE PREPARATION USING ADAPTIVE DIGITAL MICROFLUIDICS
FOR LAB-ON-CHIP DEVICES

Submitted by

Nichols Grant

Department of Electrical and Computer Engineering

In partial fulfillment of the requirements

For the Degree of Master of Science

Colorado State University

Fort Collins, Colorado

Summer 2018

Master's Committee:

Advisor: Thomas W. Chen

Edwin Chong

Brian Geiss

Copyright by Nicholas Grant 2018

All Rights Reserved

ABSTRACT

AUTOMATED SAMPLE PREPARATION USING ADAPTIVE DIGITAL MICROFLUIDICS FOR LAB-ON-CHIP DEVICES

There have been many technological advances in the medical industry over the years giving doctors and researchers more information than ever before. Technology has allowed more sensitive and accurate sensors and has also driven the size of many sensor devices smaller while increasing sensitivity. However, while many aspects of technology have seen improvements, the sample preparation of biological tests has seen lagging development. The sample preparation stage is defined here as the extracting of required features from a given sample for the purpose of measurement. A simple example of this is the solid phase extraction of DNA from a blood sample to detect blood borne pathogens. While this process is common in laboratories, and has even been automated by large and expensive equipment, it is a difficult process to mimic in lab-on-chip (LoC) devices. Nucleic Acid isolation requires common bench top equipment such as pipettes, vortexers, and centrifuges. Current lab based methods also use relatively large amounts of reagents to perform the extraction adding to the cost of each test. There has been a lot of research improving sensing techniques proposed for Lab on Chip devices, but many sensing methods still require a sample preparation stage to extract desired features. Without a complimentary LoC sample preparation system, the diversity of LoC device remains limited.

The results presented in this thesis demonstrate the general principle of digital microfluidic device and the use of such device in a small hand-held platform capable of performing many sample preparation tasks automatically, such as the extraction and isolation of DNA. Liquids are transported using a technique called Electro-wetting on Dielectric (EWOD) and controlled via a programmable microprocessor. The programmable nature of the device allows it to be configured for a variety of tests for different industries. The device also requires a fraction of the liquids lab based methods use, which greatly reduces the cost per test. The results of this thesis show a promising step forward to more capable LoC devices.

ACKNOWLEDGEMENTS

I would like to acknowledge and thank the following people for their support in this research. Without you none of this would have been possible. Dr. Thomas Chen for being a great professor and inspiring my path through electrical engineering. My incredible wife, Elizabeth, for supporting me during my long journey back to school. Other members of the BLISS lab for their insight and wisdom. My family and friends for their words of encouragement and support.

TABLE OF CONTENTS

ABSTRACT	ii
ACKNOWLEDGEMENTS.....	iii
LIST OF TABLES.....	v
LIST OF FIGURES	vi
Chapter 1 – Introduction.....	1
Chapter 2 – Background and Current Technology	3
2.1. Traditional Methods of Sample Prep	3
2.2. Analog Microfluidics	4
2.3. Digital Microfluidics (DMF).....	6
2.3.1. Fundamentals of Digital Microfluidics	6
2.3.2. Electro-Wetting on Dielectric (EWOD).....	6
2.3.3. Design and Manufacturing Considerations with EWOD	9
2.3.3.1. Breakdown	9
2.3.3.2. Resistive Forces	11
2.3.3.3. Array and Pad Design.....	12
2.3.4. Existing Digital Microfluidic Devices	15
2.3.5. Activation Signal	18
Chapter 3 – Proposed Device Design	22
3.1. Overall Device Organization.....	22
3.2. Battery and Power Distribution.....	23
3.3. High Voltage Driver.....	33
3.4. On Board Memory	37
3.5. Microcontroller	39
3.6. EWOD System Design.....	42
3.7. Position Feedback	44
3.8. User and Device Interface	49
Chapter 4 - System Implementation, Validation, and Experimental Results.....	52
4.1. System Implementation.....	52
4.2. System Validation	56
4.3. Power Supply Results	56
4.4. Position Feedback Results	60
4.5. Experimental Results	62
4.5.1. DNA Isolation	62
4.5.1.1. Immobilized Filter Method	62
4.5.1.2. Magnetic Bead Method	64
Chapter 5 – Conclusions and Future Work.....	71
5.1. Sensor Integration	72
5.2. RNA Isolation	72
5.3. PCB EWOD chip design.....	73
5.4. System Design Improvements.....	73
References	75
Appendix A – Memory Data Format.....	79
Appendix B – Device Firmware Workflow.....	80

LIST OF TABLES

Table 1 - Activation signal frequency vs movement	20
Table 2 - List of components current requirements	25
Table 3 - Feedback resistor values.....	32
Table 4 - Comparison of this research to past research. *Full protocol not completed	69
Table 5 - Protocol and volume comparison of Qiagen kit and this research	71

LIST OF FIGURES

Figure 1 - Typical NA isolation protocol.....	4
Figure 2 - a) Complete syringe pump based device. b) Disposable cartridge containing valves.....	5
Figure 3 - Typical EWOD design [24]	7
Figure 4 – Dielectrophoresis diagram [26]	7
Figure 5 - EWOD equivalent circuit [27]	8
Figure 6 - Theoretical contact angles of a droplet with and without voltage applied [29].....	9
Figure 7 - Example of droplet movement and stages (from left to right)	9
Figure 8 - Surface profile of SU-8 coating	11
Figure 9 - Droplet formations due to different pad shapes, square (a) and saw tooth (b)	13
Figure 10 - Sequence of images showing unwanted droplet splitting.....	14
Figure 11 - a) Reservoir design. b) Droplet splitting sequence [35]	14
Figure 12 - Demonstration of mixing sequence.....	14
Figure 13 - Micropump setup	15
Figure 14 - EWOD array with integrated two electrode sensor.....	16
Figure 15 - DMF platform for estrogen assays in breast tissue	16
Figure 16 - Cell culturing device containing six culturing sites in parallel	17
Figure 17 - DNA isolation for immunoassay.....	18
Figure 18 - Comparison between DC and AC signals	19
Figure 19 - System block diagram.....	22
Figure 20 - Estimated current demands through device	24
Figure 21 - The basic boost converter schematic (a), circuit when switch is closed (b), circuit when switch is open.....	26
Figure 22 - Voltage and current for each state of the control signal waveform.....	27
Figure 23 - Boost factor as a function of Duty Cycle	28
Figure 24 - Voltage division circuit.....	31
Figure 25 - Complete high voltage DC-DC boost converter circuit	32
Figure 26 - High voltage driver using pull-up resistor.....	33
Figure 27 - CMOS topology	34
Figure 28 - CMOS circuit driven by a level shifter	36
Figure 29 - Diagram of serial to parallel converter.....	37
Figure 30 - Memory structure example	38
Figure 31 - Microcontroller block diagram	40
Figure 32 – Nucleic Acid extraction chip design.....	43
Figure 33 - Position feedback equivalent circuit	46
Figure 34 – Position feedback with half wave rectifier circuit	47
Figure 35 - ADC voltage reference (AREF) obtained by voltage division.....	48
Figure 36 - SNR for fixed reference voltage and through voltage division	49
Figure 37 - Side view of PCB and battery showing placement relationship.....	52
Figure 38 - PCB layout by functional blocks.....	53
Figure 39 - Finished and populated circuit board	54
Figure 40 - a) Compression connector b) Complete EWOD chip adapter board with compression connector array ..	55
Figure 41 - Complete device showing EWOD chip loaded. a) Closed b) Open.....	56
Figure 42 – Lithium ion battery discharge curve.....	57
Figure 43 - Charging curve for lithium ion battery.....	58
Figure 44 - 5V SMPS output during power on and off.....	58
Figure 45 - Current draw from High Voltage circuits	59

Figure 46 - Vsense results for multiple cycles of movement.....	60
Figure 47 – EWOD design for filter method	62
Figure 48 – a) Capture area showing fluorescents after wash. b) Waste reservoir after wash. c) Output of device in Eppendorf tube.	63
Figure 49 - Plate reader results of DNA Filter protocol	64
Figure 50 - Unbound DNA for volume of beads	65
Figure 51 - EWOD device for Magnetic Bead method	66
Figure 52 - Theoretical magnetic field lines a) without fieldguide and b) with fieldguide.....	67
Figure 53 - a) Sample reservoir. b) Waste reservoir with unbound DNA. c) Output reservoir with eluted DNA.	67
Figure 54 - Plate reader results of Magnetic Beads protocol.....	68

CHAPTER 1 – INTRODUCTION

With the increasing computing power and shrinking size of modern microprocessors, bio-medical devices have benefited tremendously from the advances in computing power and other technological advances. Researchers are able to gather data that was once limited only to the most advanced tech labs. Additionally, processes that were once only available inside of labs are finding their way into smaller devices tailored to the average user. Glucose meters may be one of the best examples of how modern technology made glucose testing readily available and easy to use for diabetic patients. Modern glucose meters can easily fit in your pocket and are battery powered for portability. The sensor technology in glucose meters is not trivial, yet they are relatively inexpensive. Maybe the most intriguing developments, with respect to this research, are the current Point-of-Care (PoC) devices for medical use [1]–[3]. Products such as i-STAT from Abbott [4] give nurses and doctors more diagnostic information than they had before. However, the capability to directly detect disease is extremely hard to develop. Any care provider attempting to confirm a diagnosis of a blood borne pathogen must turn to a laboratory specialized in processing such sample types. Most modern hospitals in the U.S. offer best case scenarios where a biological lab is typically in-house providing results back in about 24-48 hours. In other industries, other locations, or if the lab is external, results could be delayed several days. Any delay in results delays the diagnosis and treatment of a patient, which in many cases can do catastrophic damage to organs or be life threatening. Many infectious diseases such as Ebola, Zika, and Malaria have become wide spread in different parts of the world, and fast detection of such diseases would be helpful in responding to outbreaks. With Point-of-Care devices being common place and the price of computing power continuing to drop, one might expect that tests such as pathogen detection would be available by now. However, current PoC devices have stopped short of offering the majority of test done in a lab, partially due to the challenges of providing sample preps on the same PoC platform.

The process of detecting a disease in the body can typically be broken into two major steps. A “sample preparation” step to extract the features trying to be measured, and a “sensing” step to provide detection information about the feature. The details of each step can take on many forms. However, there tends to be at least one step where the sample is combined with another reagent for the purpose of sensing. For pathogen detection, most sensing techniques rely on the detection of either DNA or RNA, which means these features need to be extracted from the

cells in which they reside. Once the nucleic acids have been recovered from the sample, they are typically amplified using a Polymerase Chain Reaction (PCR) [5]–[8] machine. Specific nucleic acid strands are identified using an appropriate tag containing Green Fluorescent Proteins (GFP), where fluorescent intensity readings are then recorded using a plate reader. The final step of using the plate reader to detect fluorescent intensities is an example of sensing. Developments have been made in sensor technology to offer alternatives to the large bench top equipment, such as the PCR and plate reader, used in labs. Research in sensors has shown options that are well suited for PoC devices, in terms of size, cost, and simplicity [9]–[11]. However, they still fundamentally rely on the nucleic acids to be available. The sample prep stage, however, remains a difficult challenge as it typically requires bulky equipment such as pumps and centrifuges. While versions of the benchtop equipment have been made to greatly reduce the size of each component, they are still too large for a hand held device suitable for PoC applications. Even if the size could be reduced further, there are also issues of flow control and functionality. Without a solution to the issue of preparing samples on a small scale, the capability and development of PoC devices will remain limited.

In this thesis, a sample preparation device that can be used in a hand held PoC device is proposed. Droplet manipulation uses a process of Electro-Wetting on Dielectric (EWOD), which is capable of moving a variety of liquids. A removable chip is designed to store required reagents, mix appropriate volumes, and separate liquids according to the assay being performed. An electronic control system consisting of on board memory, microcontroller, and high voltage drivers manage the order and timing of the droplet movement according to the assay protocol. All power consumption is kept low enough to be operated from a lithium ion battery. The entire system size is kept small enough to easily integrate into a hand held PoC device. By enabling automated sample preparation on such a small scale, the ability of having lab tests performed on a hand held device can become a reality.

CHAPTER 2 – BACKGROUND AND CURRENT TECHNOLOGY

2.1. TRADITIONAL METHODS OF SAMPLE PREP

All electrical sensors are designed to detect a specific feature and translate its findings into electrical signals. A microphone detects sound waves, photodiodes detect light intensity, etc. It is assumed that the sensor will be used in an environment where these features are available for detection. For instance, a traditional microphone is not expected to work in the vacuum of space, and the photodiode is not expected to detect light in a closed box. If the features the sensor detects is not available, no data will be obtained from the sensor. The concept of having features available for detection is not as trivial in biological matters. Much like the outer layer of the earth's atmosphere defines a barrier between where sound waves travel and the vacuum of space, the body has its own protective barriers such as skin, organs, and cells which create a separation between very different environments. Each barrier also separates different features, making for very different sensing opportunities depending on which environment is being analyzed. The skin barrier is the reason a glucose meter needs a blood sample to detect glucose. The wall of a cell is a barrier, and the reason current PoC devices cannot detect blood borne pathogens directly and easily.

The current lab based methods for detecting viruses in a sample typically rely on the detection of the viral DNA or RNA. Both DNA and RNA are found inside of cells and, therefore, also inside of the bacteria and viruses living inside of the body. For a sensor to detect the presence of DNA or RNA, the sensor must either be placed inside of the cell or, more likely, the cells opened to release the Nucleic Acids (NA)s. Commonly, either DNA or RNA is isolated from the sample by breaking open all cells found in the sample (lysis), trapping the nucleic acids, washing, and releasing (eluting) the DNA. In general, this process is referred to "sample preparation" [12]–[14]. Many manufacturers of biological equipment and reagents sell kits specific to performing various types of sample prep that come with the appropriate reagents and special equipment. For instance, Qiagen sells the Nucleotide Removal Kit [15] that can be used to isolate DNA from a blood sample. The kit comes with three reagents, a package of NA binding filters, and instructions detailing how to perform the sample preparation. In a typical lab, a trained lab technician will prepare the sample according to the kit instructions before transferring the results to other bench top equipment for analysis.

Figure 1 shows a common protocol used to isolate DNA from a given sample. A trained lab technician will pipette a specific volume of sample into a container, followed by a lysing reagent at a ratio specified by the instructions. The lysing buffer will break open all cells found in the sample releasing all NAs that were contained within the cells. The DNA solution is then transferred to a supplied column containing the binding filter and placed into a centrifuge to spin down. The centrifuge forces the solution through the binding filter which traps the DNA along with residual material such as cell wall fragments, proteins, etc.

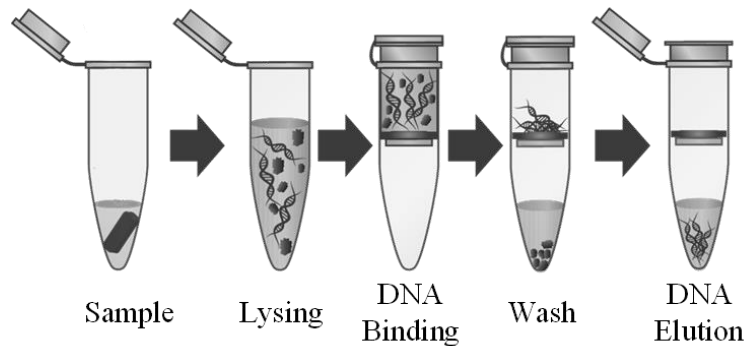


Figure 1 - Typical NA isolation protocol

A wash buffer is then added to the column to help rinse away all unwanted debris while leaving the bound DNA. Again, a centrifuge is used to push the wash buffer through the filter. Finally, the waste is discarded and an elution buffer is added using a pipette and centrifuged through to release the DNA from the filter. The isolated DNA solution can then be analyzed using equipment appropriate for the assay. The isolation of NAs can be easily automated in a laboratory setting using robotic arms and pipettes, however, this is completely impractical for PoC testing.

2.2. ANALOG MICROFLUIDICS

Microfluidics is a term that describes the movement of small amounts of liquid (sub mL). It has long been used inside of labs to transport liquids during an assay, and can take many forms. While a pipette can dispense a single, specific, volume, it cannot provide continuous flow. Additionally, pipettes are hand held making precise placement of liquids challenging. Microfluidics can deliver an accurate continuous flow of a small amount of liquids to a precise location through small (sub mm) channels or tubing. Adding valves introduces a method to direct flow through any number of channels enabling experiments to be done in parallel. While the continuous flow of reagents can increase throughput of certain experiments, it is at the cost of system size. The common way to pump liquids through a

microfluidic system is a syringe pump, which compresses a standard medical syringe at a user defined rate. The syringe is then connected to the microfluidic tubing which delivers the liquid to the experiment. T. Baier et al [16] combined the syringe pump with capillary techniques to create an automated sample preparation device to extract nucleic acids from a given sample. The pressure from the syringe pumps were diverted to different channels using custom made valves which add to the practicality of the device, but also the complexity. Figure 2 shows the syringe pump based device (a) and its disposable cartridge which contains the reagents required for the assay. The device is compact in terms of lab bench style equipment, but it is far from being a device which is capable of being hand held or battery operated.

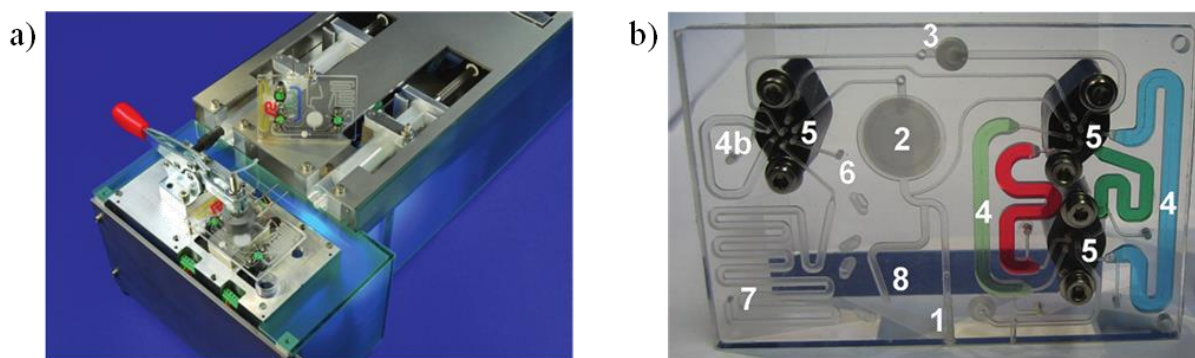


Figure 2 - a) Complete syringe pump based device. b) Disposable cartridge containing valves.

While the paths of the liquids can be modified to suit other assays, the position of the valves, number of syringes, etc., limit the device's versatility. Additionally, the device still uses a relatively large amount of liquids compared to other microfluidic designs.

Other types of microfluidics are paper / capillary [1], [17]–[21] and blister packs. Each of these can be made extremely small, but lack control of the liquid. Similar to the syringe pump, the liquid simply follows a predetermined path, and flow rate is dictated by the capillary forces on the liquid. Again, more complex tasks such as mixing fluids is difficult with capillary type microfluidics. Blister packs do have an advantage of being able to pressurize the channels which can help force the liquid through obstacles or filters, increasing the functionality of the microfluidic system. However, the pressure is only a quick pulse at the beginning and is inconsistent due to process and human variations. One major disadvantage of capillary type microfluidics is that the liquid cannot be stopped on demand which leads to vary inaccurate volumes being drawn.

The syringe pump has its uses in the lab, but is not practical for PoC devices due to the relatively large size of the pump motors and screw drive. Additionally, syringe pumps are limited in the control over the liquid, which are ideal for pushing or drawing fluid, but lack the ability to do more complex tasks such as mixing. Furthermore, if the assay requires multiple reagents, then multiple pumping mechanisms would be required, only adding to the size and complexity of the device. Capillary microfluidics has its place in assays where little to no sample prep is needed. Typically, this presents a situation where it is desirable to draw in as much of the sample as possible. Hence, they have found widespread use in PoC devices such as pregnancy tests and glucose meters. However, if a sample preparation stage is needed, which typically require specific volumes and ratios, a device with more control is mandatory.

2.3. DIGITAL MICROFLUIDICS (DMF)

2.3.1. FUNDAMENTALS OF DIGITAL MICROFLUIDICS

The above examples might be considered *analog* microfluidics due to the lack of any digital control or movement method. However, there does exist its compliment, Digital Microfluidics (DMF), which offers much more control over liquid movement. DMF is typically implemented using a process called Electro-wetting on dielectric (EWOD). The process of EWOD is not new and has been researched for many years moving many materials [22][23]. The Electro-wetting on Dielectric (EWOD) design offers the ability to accomplish all of these tasks, and this thesis addresses specific design aspects as well as challenges encountered in developing practical applications.

To be an effective sample preparation device, the system must be able to perform three basic operations:

- Transport – The movement of a droplet from point A to B.
- Split – Separating a smaller volume from a larger volume.
- Mix – The ability to homogenize two different liquids.

2.3.2. ELECTRO-WETTING ON DIELECTRIC (EWOD)

Electro-wetting on Dielectric is a way to move liquids using voltage, allowing more control over the liquid than other microfluidic methods. Figure 3 shows the typical EWOD system design commonly referred to as a “closed” or “two plate” configuration. Below the droplet is an array of conductive electrodes covered by an insulating material and hydrophobic layer. Above the droplet is a single conducting plane with a hydrophobic layer. Applying a voltage to one of the bottom conductive pads, adjacent to the droplet, attracts the droplet to the active pad. Between the plates,

the droplet can be surrounded by a dielectric media, such as silicone oil or air. The combined assembly of the top and bottom plates of the EWOD system is referred to in this paper as a *chip*.

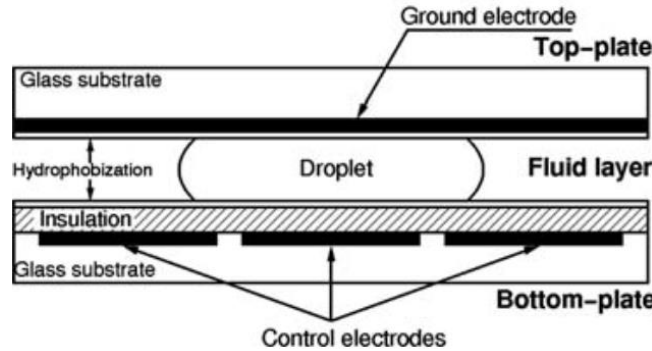


Figure 3 - Typical EWOD design [24]

The main principle that contributes to the movement of the droplet is dielectrophoresis (DEP). When a droplet is exposed to a non-uniform electric field, such as in Figure 4, the difference in charge concentration on either side of the droplet causes a net force in the direction of the more concentrated charge. The force on the droplet can be quantified by the equation below [25] (Equation 1).

$$F = \frac{dU}{dx} = \frac{d}{dx} \left(\frac{1}{2} cV_n^2 + \frac{1}{2} cV_p^2 \right) = \frac{1}{2} \frac{\epsilon_n - \epsilon_p}{h} AV^2 \quad (1)$$

Where V is the voltage applied to a pad, ϵ is the equivalent permittivity of the insulating layer and droplet, h is the distance of the top plane from the bottom. The n and p subscripts represent the areas of the droplet that are positively and negatively charged.

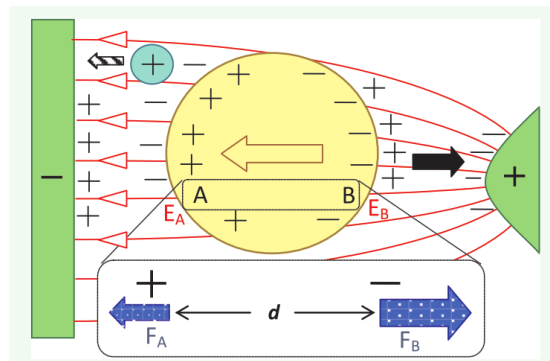


Figure 4 – Dielectrophoresis diagram [26]

Figure 5a shows the equivalent circuit of the two plate EWOD design. Each of the dielectric layers form a capacitor, C_i for the insulating layer, C_h , for the hydrophobic layer. When the droplet is not present above the pad, the equivalent capacitance is based on the dielectric media being used (C_m). If the droplet exists over the active pad, the equivalent circuit becomes a capacitor and resistor in parallel due to the droplet being conductive. Equation 1 is based on the difference in capacitive energy between the equivalent circuit formed above the active pad vs the grounded pad. The capacitance of the dielectric and hydrophobic layers are governed not only by the permittivity of the dielectric materials used, but also by the area over the droplet covering the active pad (Figure 5b).

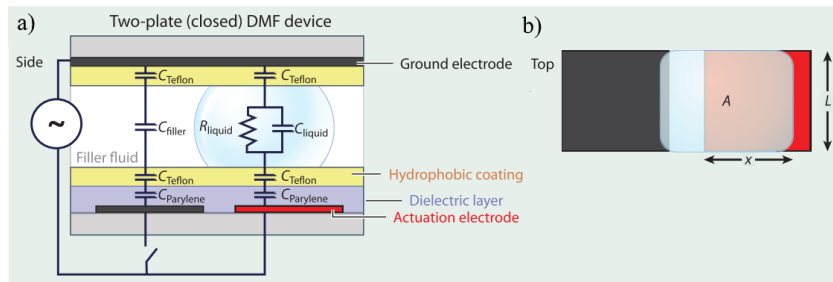


Figure 5 - EWOD equivalent circuit [27]

The forces acting on the droplet can be seen through the change in contact angle of the droplet when the voltage is applied (Figure 6). Contact angle is measured at the interface of the hydrophobic and droplet surfaces through the droplet as shown in Figure 5. When a voltage is applied, the DEP forces draw the droplet closer to the hydrophobic surface, lowering the contact angle. The lower contact angle suggest that capillary force plays a role in moving the droplet as well, however, its significance has been argued [28]. This thesis puts the focus on the DEP forces and considers contact angle and capillary forces a second order effect.

Figure 7 shows an example of droplet movement from left to right. Most liquids move to an adjacent pad following the stages listed in Figure 7 where “Start” is simply where droplet movement is initiated. The shape of the droplet is typically round if no activation voltage has been applied. “Elongation” happens when the pad adjacent to the starting position is activated, drawing the droplet to the activated pad. A “Tail” is usually created as the majority of the force on the droplet is acted on forward facing side. The tail of the droplet lags behind since it is pulled due to surface tension of the droplet material. Once the droplet reaches the active pad, the sequence is considered finished when the tail of the droplet has also reached the active pad.

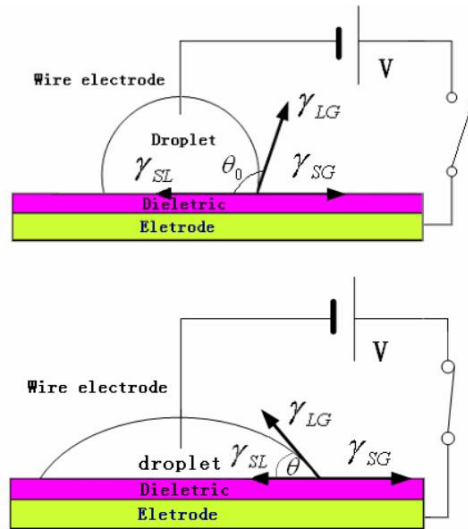


Figure 6 - Theoretical contact angles of a droplet with and without voltage applied [29]

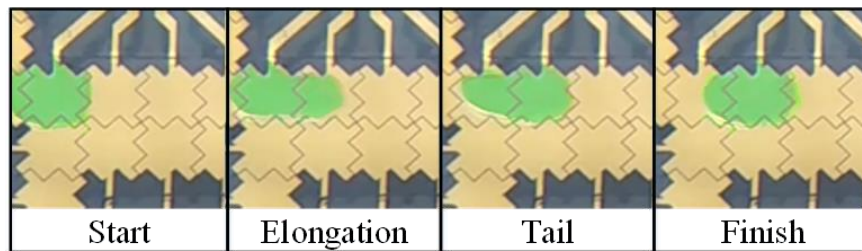


Figure 7 - Example of droplet movement and stages (from left to right)

2.3.3. DESIGN AND MANUFACTURING CONSIDERATIONS WITH EWOD

2.3.3.1. BREAKDOWN

Breakdown is the term given to the process of a dielectric material becoming conductive. Breakdown irreversibly damages the dielectric layer, and inherently, the hydrophobic layer. The damage can make it impossible for the droplet to move for a couple of reasons. First, because the dielectric has become conductive, this prevents the accumulation of charge to build around the active pad. Secondly, the damaged hydrophobic layer adds friction that resists droplet movement. It can be seen from Equation 1 that the force depends on both voltage and capacitance, but trying to increase the force by increasing these parameters can put these parameters at odds with each other. Equations 2 and 3 shows the relationship between the voltage across a capacitor and the charge collected on its surface. Increasing the charge on the dielectric layer increases the force on the droplet. In an EWOD system the voltage on the active pad held constant. Therefore, the charge is governed by the capacitance of the dielectric layer. Equation 3 is the equation

for a parallel plate capacitor where ϵ is the permittivity of the dielectric, A is the area, and t is the thickness of the dielectric layer. Decreasing the dielectric thickness will increase the capacitance, and in turn increase the charge on the surface, and the force on the droplet. Dielectric strength is the maximum electric field the dielectric material can withstand before it becomes electrically conductive. Since the electric field can be considered voltage per distance ($V/\mu\text{m}$), the maximum voltage a dielectric layer can withstand is its dielectric strength multiplied by the layer thickness. Hence, lowering the thickness of the dielectric layer will lower the voltage it can withstand. Increasing the dielectric thickness would increase the maximum voltage the dielectric layer can support, however, it is in conflict with the desire to decrease the thickness to raise the force on the droplet.

$$Q = CV \quad (2)$$

$$C = \frac{\epsilon A}{t} \quad (3)$$

Many experiments were done with different materials and thicknesses and this conflict was experienced. The activation voltage of the droplet has to be large enough to overcome the resistive forces of the media being used. Experimentally, it was found 80V – 100V was sufficient for all reagents used, which is consistent with other research [30][31][32]. With the droplet being a conductive material, much of the voltage from the active pad is across the insulating layer between the droplet and active pad. Therefore, the dielectric strength of the insulating layer needs to withstand the activation voltage. In practice dielectric breakdown became a challenge to address due to inconsistent dielectric strength specifications and manufacturing processes. Figure 8 shows profilometer results from two different pad arrays and a dielectric layer of SU-8. The readings were adjusted from side to side to align correctly. The dips in the ‘CrAu 1,2’ plots are the gaps between pads. The SU-8 layer was applied using a spin coater (described later), but a dip matching the pad gap remains on the SU-8 surface. The dip in the surface profile causes a weak area along the edge of the pad. This effect was seen when using Polydimethylsiloxane (PDMS) as well and seems to be a symptom of spin coating textured surfaces. Parylene-C was also tested and applied using a vapor deposition process which theoretically coats the surface evenly, even if it is vertical. However, in practice it was found the vapor deposition process could leave small pin holes in the dielectric layer at thicknesses below $2\mu\text{m}$. With these variances the maximum voltage of the active pad should remain much lower than what would be calculated based on the dielectric strength of the insulating material.

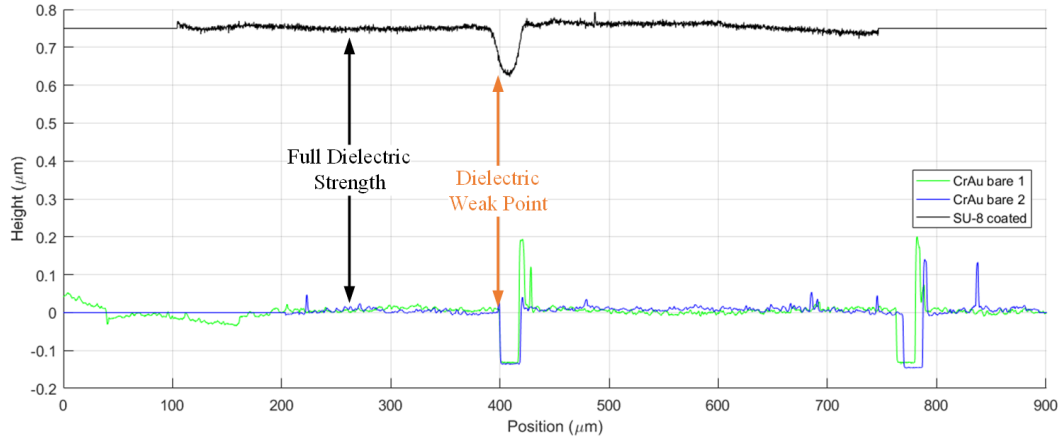


Figure 8 - Surface profile of SU-8 coating

The issue of breakdown can be a challenging symptom to diagnose. However, the insulating layer became one of the most significant factors in creating a reliable EWOD system. For instance, Parylene-C has a dielectric strength of $220\text{V}/\mu\text{m}$, and with a thickness of $2.0\mu\text{m}$ makes the theoretical maximum activation voltage 440V . Despite such a high breakdown voltage, breakdown was still an issue with activation voltages as low as 80V due to the pin holes mentioned earlier. In contrast, SU-8 has a dielectric strength of $112\text{V}/\mu\text{m}$ and with a thickness of $2.0\mu\text{m}$ the breakdown voltage is 224V . Again, breakdown was still an issue at activation voltages as low as 80V . However, it was determined that this was due to the issue described in Figure 8. Finally, to avoid pin holes in the dielectric layer of Parylene-C, a thickness of $2.5\mu\text{m}$ was used, making the breakdown voltage 550V . However, the lack of pin holes and forming a uniform surface contributed most to the resistance to dielectric breakdown. During device tests, activation voltages have reached $\sim 100\text{V}$ without breakdown issues making for an extremely reliable EWOD system.

2.3.3.2. RESISTIVE FORCES

The environment that the droplet will move in can make a large difference in the performance of the EWOD system. As stated before, the movement of the droplet is the result of the difference between the dielectrophoresis force and the resistive forces of the system. One way to improve EWOD system performance is to increase the dielectrophoresis forces as previously discussed. Another aspect is to reduce the forces trying to resist the movement of the droplet. As seen in Equation 1, there is an opposing force due to the concentration of charge opposite of the active pad. The force is less due to the lower concentration of charge compared to the active pad. However, there isn't much of a way to control charge concentration of the grounding surface independent of the active surfaces. Resistive forces also come from the interface between the droplet and the surrounding surfaces in the form of drag. The first

step to reduce drag is the application of the hydrophobic layer over the insulating layer. Different hydrophobic layers were tested including Teflon, Rain-X, and peanut oil [33]. Each of these materials made it possible to move liquids, but Teflon was preferred due to its low thickness, ease of application, and durability. The next feature that can be adjusted to reduce drag is the media the droplet moves in.

Our early attempts to move droplets in this research were done in air. However, the use of peanut oil as a hydrophobic layer, as well as other research [32], gave insight into other media that could be used to submerge the EWOD system and reduce the drag on all sides of the droplet. While media such as oil reduces drag by keeping a thin layer of oil between the droplet and the hydrophobic surface, it introduces a new concern in term of viscosity. Oil is inherently harder to displace than air, so it is important to use a very low viscosity oil such that it mimics air as much as possible. Silicone oil is a commonly used media [31] as it is readily available in low viscosity forms, and was the preferred choice in this research. Other medias were tested such as mineral oil, but the viscosity is high enough to prevent droplet movement.

Another advantage of using a media other than air is to reduce evaporation of the materials being moved. The tests done in this research moved volumes 100nL – 200nL which would evaporate within minutes in air. Additionally, the tests in this research can take much longer than the time it takes for the liquids to evaporate. Using a media such as silicone oil can help prevent evaporation for hours.

2.3.3.3. ARRAY AND PAD DESIGN

There are several aspects of the pad array design such as pad shape, thickness, and spacing between pads that affect EWOD system performance. As discussed earlier, the DEP forces acting on the droplet are from the charge concentration on the active pad. It is worth noting that if the droplet is not close enough to the active pad then the force from the electric field will not be large enough to move the droplet. Therefore, reliability is increased if the pads are positioned as close to each other as possible. To make the EWOD system as reliable as possible a photolithography process was selected to create the pad array since it can offer features as small as 10 μ m.

An obvious pad shape would be a simple square which is not uncommon to see in other literature [31]. However, the DEP forces are strong enough to force the droplet to take the shape of the active pad (Figure 9a). In theory the droplet will still move to the next pad when activated, however, in practice the droplet may not end up close

enough to the next pad for the DEP forces to act on the droplet. The farther away the droplet is from the activated pad, the higher the activation voltage needs to be to initiate movement [34]. Other pad designs offer more consistent movement such as the saw tooth design in Figure 9b. The shape taken by the droplet is similar to the square, but overlaps the adjacent pads. Having a slight overlap helps get the forces from the active pad closer to the droplet than what would be possible with a simple square.

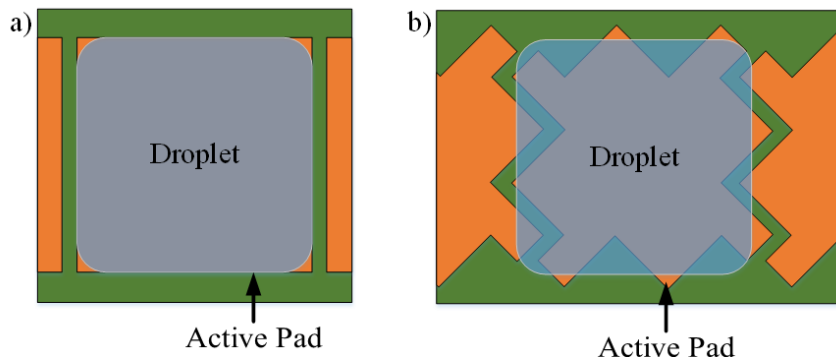


Figure 9 - Droplet formations due to different pad shapes, square (a) and saw tooth (b)

Thickness of the pad array can impact the EWOD performance as well, although, maybe not in a way that is obvious. Figure 8 suggested that the gap between pads is translated to the surface even though a coating has been placed over the conductive material. One might expect the gaps to be fill, and the surface completely smooth. However, it can be seen in Figure 8 that that depth of the dip in the surface is nearly as deep as the gap between the pads. Vapor deposition does not improve the surface profile since it follows the profile of the substrate even closer. Increasing the thickness of the conductive material only exaggerates this effect, and makes the dip in the surface even deeper. However, in experiments the added surface roughness did not seem to significantly impair movement. Instead, a design with relatively thick conductive pads resulting in a deep trough in the surface profile, can cause unwanted splitting of the droplet during movement. Figure 10 is a sequence of images attempting to move a droplet from left to right. The droplet is being moved in silicone oil on a pad array made from a printed circuit board (PCB) with a Parylene-C dielectric layer. The copper thickness was 1.5oz (~150 μ m) resulting in roughly the same gap in the surface profile after Parylene-C coating. The deep gap between pads was enough to restrict a portion of the droplet causing it to split instead of moving the entire volume. The photolithography process allows for sub μ m thick conductive layers to be applied to the substrate reducing the risk of unintended splitting.

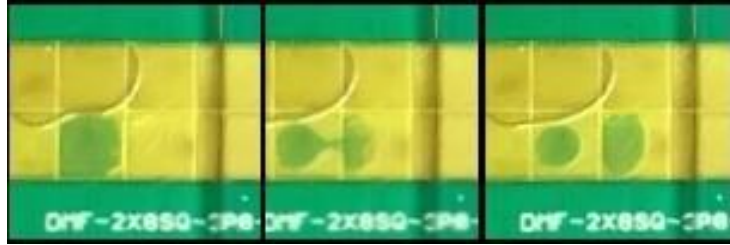


Figure 10 - Sequence of images showing unwanted droplet splitting.

Any EWOD system designed for sample preparation must contain areas appropriate for their intended use. To be able to move droplets, there first needs to be liquids loaded into the EWOD system. Therefore, pads designed to act as reservoirs are useful to split appropriate sized volumes for the assay. Figure 11a shows a reservoir design typical of other research. The diameter of the reservoir can be changed to accommodate the volume of reagent used for the assay. Figure 11b shows how the reservoir and accompanying transport pads split a droplet from the larger reservoir volume.

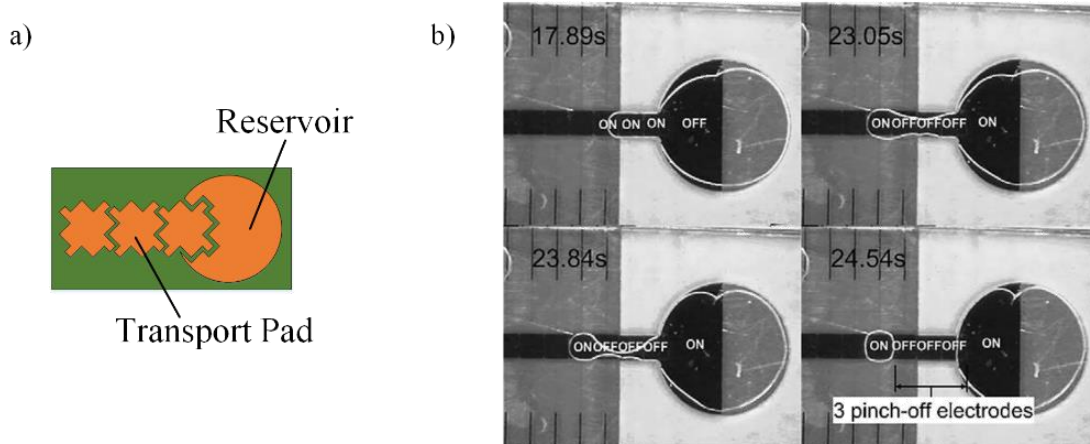


Figure 11 - a) Reservoir design. b) Droplet splitting sequence [35]



Figure 12 - Demonstration of mixing sequence

Another requirement of a sample preparation system is the mixing of liquids. To mix droplets in the EWOD system, two different liquids can be brought together and the larger volume moved in circles until homogenous. By creating an array of transport electrodes allows enough room to mix the volume appropriately. Figure 12 shows an example of the design used in the our research mixing two liquids in a small mixing area constructed of an array of transport electrodes. A variety of assays can be performed by mixing and matching these designs together in one large EWOD system.

2.3.4. EXISTING DIGITAL MICROFLUIDIC DEVICES

Over the years DMF has been researched for many applications including cell culturing, impedance spectroscopy, and immunoassay. An example of a basic DMF is demonstrated in research by M. Paknahad et al [36] where a droplet is moved along a series of 8 electrodes with the purpose of demonstrating and characterization of the design.

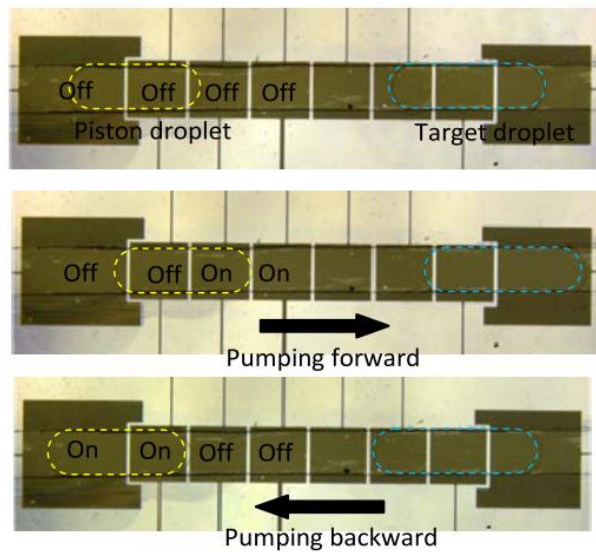


Figure 13 - Micropump setup

These setups are common in early research of EWOD systems and often only use De-Ionized (DI) water as their liquid material. It will be seen that these setups are “ideal case scenarios” and do not necessarily translate to other designs or liquids. J. Gong and C. J. Kim [32] demonstrated an EWOD system which consists of 8x8 electrode array which greatly improves the capability of the device. However, no practical assay was performed and only DI water was used to demonstrate functionality.

A demonstration of impedance spectroscopy was performed by T. Lederer et al [37] which shows the intriguing integration of a two electrode sensor with a DMF system. Integrating a sensor suggests several possibilities for a DMF system including electro-chemical and affinity sensors. However, since the focus was primarily impedance spectroscopy the device as a whole lacks investigation of many liquid types and other aspects that contribute to its functionality.

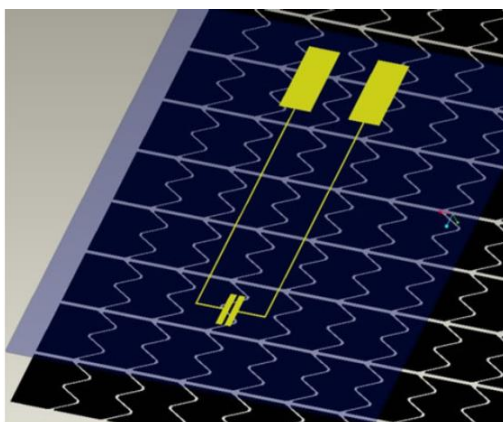


Figure 14 - EWOD array with integrated two electrode sensor

A more practical example was done by N. A. Mousa et al [38] where an estrogen assay was performed on an EWOD system containing a total of 34 electrodes moving multiple liquids, including blood.

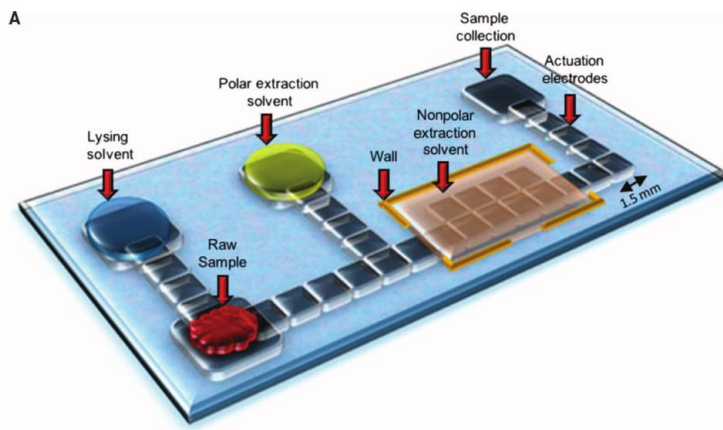


Figure 15 - DMF platform for estrogen assays in breast tissue

Although many assays require the manipulation of more reagents and the protocol is relatively simple in terms of number of positions moved. Another example of a practical assay performed on an EWOD system was by S. Shih et al [39] showing automated cell culturing device. A major advantage of the EWOD design is the extremely

small size which allowed six culture sites to be integrated in parallel while still maintaining a small form factor. While movement and cell culturing was well demonstrated, attention is given to supporting elements needed in a real application.

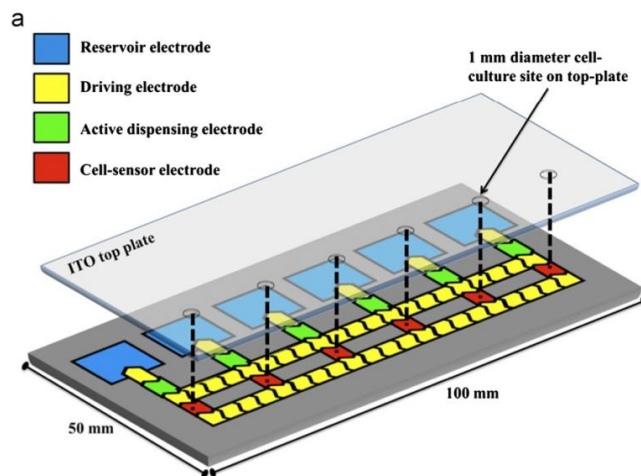


Figure 16 - Cell culturing device containing six culturing sites in parallel

For instance, loading and unloading of reagents and cells is done during the assembly and disassembly of the device. Since the primary focus of DMF research is typically discovering if a certain process can benefit from DMF, loading and unloading liquids understandably gets overlooked. Additionally, cells were cultured at 37° C with 5% CO₂. The systems providing these conditions were not integrated, therefore, requiring external equipment.

An immunoassay demonstration was done by P. Y. Hung et al [22]. DNA was extracted from whole blood requiring the movement and mixture of five reagents on a system conducted over 13 electrodes. However, magnetic beads were used to extract the DNA, but an elution of the DNA was never performed. Additionally, the application of the magnet to attract the magnetic beads seems to be done manually which detracts from the validity of the device's full capabilities.

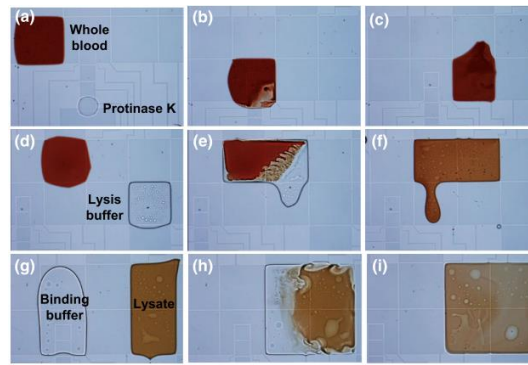


Figure 17 - DNA isolation for immunoassay

2.3.5. ACTIVATION SIGNAL

Up to this point the activation voltage has been discussed and mentioned to be between 80V-100V, but what has not been discussed is a way to deliver the appropriate voltage to the desired pad and in what form the signal should take. Dealing with voltages as high as this is not a trivial matter. Especially when attempting to power such a system off of a battery.

There are two major domains in which an activation voltage can be delivered, Direct Current (DC) or Alternating Current (AC). When applying a DC activation signal, charge is applied to the active pad until the activation voltage has been reached. The activation voltage is to be held steady until the controller changes which pad is active. In other words, the activation voltage is not intended to fluctuate while the droplet moves to the active pad. However, it is not necessary for the activation voltage to remain steady, and an AC signal can be used. An AC signal suggests that the voltage is going to fluctuate in some predefined manner. If an AC signal is used, then there is the choice of several waveforms. Figure 18 shows the difference between a DC signal and two different AC waveforms. It can be seen by the magenta signal in Figure 18 (V_{DC}), that the DC signal does not change over time. However, the AC signals shown in the lower portion of Figure 18 change voltage periodically. A pure AC signal is symmetrical about the 0V (ground), and the amplitude is measured from 0V to the maximum value the signal reaches. A defining characteristic of an AC signal is the periodicity of the signal. Each of the waveforms in Figure 18 repeats, where one unique pattern is a *cycle*. The number of cycles completed in one second is *frequency* which uses the unit Hz (cycles/s). For reference, Each of the AC signals in Figure 18 have a frequency of 1kHz. A common waveform in many applications is the sine wave, shown as the blue signal in Figure 18 (V_{SINE}). In the example in Figure 18, the sine wave has an amplitude of 30V, meaning that the voltage fluctuates between -30V and +30V. Another common waveform is the square wave,

shown as the red signal in Figure 18 (V_{SQUARE}), which has an amplitude of 50V. It is also possible to add signals together to produce a more complex waveform. When signals are added, their instantaneous values are simply added at each time point. Similarly, complex waveforms can be separated into their unique components. For instance, if the square wave of Figure 18 can be added to the DC waveform in Figure 18. The result is the cyan waveform in Figure 18 ($V_{\text{SQ+DC}}$). The magnitude of the DC signal is 50V, which therefore gets added to the square wave. The 50V DC component shifts the square wave up by 50V. Therefore, the resulting waveform is a square wave that fluctuates from 0V-100V, instead of -50V to +50V.

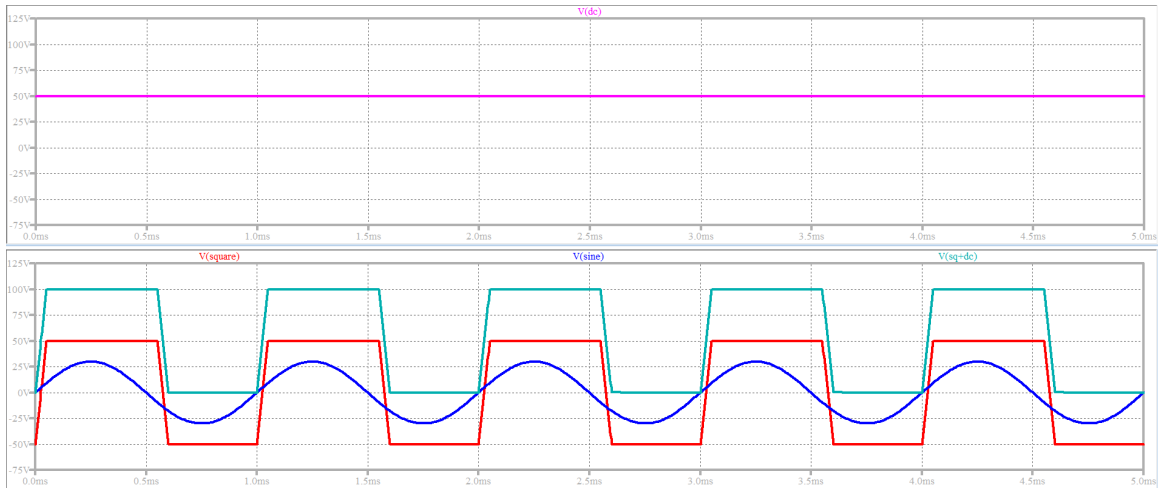


Figure 18 - Comparison between DC and AC signals

It can often be helpful to think of a given waveform as the components that make up that waveform. For instance, in the $V_{\text{SQ+DC}}$ example, it can be helpful to recognize that there is a DC component that exists, and can be treated separately. Square waves that fluctuate between 0V and some higher voltage are common in digital circuits and are referred to in this paper as a *pulse wave*. It should be obvious that AC signals spend less time at their peak voltage compared to DC signals. Equation 4 shows the derivation of the Root Mean Squared (RMS) voltage of a square and pulse wave. It can be seen that V_{RMS} depends highly on the signal's duty cycle (D), and indeed typically less than DC.

$$V_{rms} = \sqrt{\frac{1}{T} \int V_p u(t)^2 dt} = \sqrt{\frac{1}{T} \int_0^{t_{on}} V_p^2 (1)^2 dt} = \sqrt{\frac{1}{T} V_p^2 (t_{on} - 0)} = \sqrt{V_p^2 D} = V_p \sqrt{D} \quad (4)$$

The duty cycle of a signal is a percentage of time (t_{on}) the signal is at its peak voltage (V_p) versus the period of the cycle (T). The duty cycle can be summarized as $D = t_{on}/T$. Other research has used either DC, pure AC sine wave, pure AC square wave, or a pulse wave with EWOD systems [22][28][34][40]. It has been shown that lower frequencies result in higher DEP forces [28], but experimentally, it was found that AC signals are better at maintaining droplet movement despite effects of breakdown. A simple movement test was conducted to understand if there were any significant differences between signal types. A program was made to transport a droplet of deionized (DI) water back and forth across a sequence of pads. A pulse wave with an amplitude of 100V was applied to the appropriate pad in the sequence for 0.5s. if the activation signal was strong enough the droplet moved to the active pad. If the activation signal was not strong enough to move the droplet, the droplet would remain at the previous pad. The only aspect of the signal that was changed was frequency, and Table 1 summarizes the results.

Freq. (Hz)	Speed	Movement
0 (DC)	Fast movement.	Breakdown stopped movement.
1,000	Similar movement to DC.	Previous breakdown stopped movement.
2,000	Slower movement than previous frequencies.	Intermittently moves across breakdown area.
3,000	Slower movement than previous frequencies.	Consistently moves across breakdown area .
5,000	Slower movement than previous frequencies.	Consistently moves across breakdown area.
10,000	Slower movement than previous frequencies.	Previous breakdown stopped movement.

Table 1 - Activation signal frequency vs movement

All frequencies were tested using the same EWOD chip, so damage done from the previous frequencies would remain for later frequencies. The first frequency that was tested was 0 Hz (DC) which caused the droplet to move instantaneously to the active pad. Since the active pad was activated for 0.5s, the droplet remained over the active pad while the activation time finished. During this time, over one of the pads in the sequence, breakdown started to happen. As stated previously, breakdown can damage the dielectric layer and surface, which prevented the droplet from moving any further. Interestingly, as the frequency of the activation signal was increased, the droplet was able to move over the damaged area. However, as the frequency was increased, the droplet became harder to move. The ability for AC signals to perform better over breakdown damaged areas is curious. Other research has seen improved droplet mobility using AC signals vs DC as well [24]. One may consider that since the RMS voltage of the signal is

less than DC, then the effective voltage is lower and not exceeding the max dielectric voltage of the dielectric material. However, dielectric strength is not a function of RMS or average voltage. Instead it is solely dependent on the peak voltage of the signal at any given time. Therefore, even though the RMS voltage of a pulse wave may be below the max voltage of the dielectric material, it is possible the peak voltage of the waveform exceeds the dielectric strength.

In summary, traditional analog microfluidics are a good addition to in-house laboratories where large equipment is already in use. They can be very versatile and offer features such as continuous flow to create experiments more difficult otherwise. However, the goal of the proposed device aims to reduce the need of a lab by offering testing abilities in the field, where the samples are taken. Analog microfluidic solutions have their limitations to become as small as needed or as diverse as needed to be practical for PoC testing. Digital microfluidics shows great promise, but demonstrations found in existing research have been relatively simple, only requiring a small number of movements and mixing of few reagents. These demonstrations are adequate to display the very basics of DMF but tend to leave out areas of weakness in the designs. The low complexity of the assay, number of movements and reagents inherently mask potential reliability issues since the chance for something to fail is also low. If proposing that an EWOD system can be used for PoC devices, it must be shown that EWOD is a reliable and capable process. This thesis demonstrates a complete process of extraction and isolation of DNA from a sample on a small, battery powered, EWOD device to show the potential of digital microfluidics technology. The assay being completed requires nearly 500 movements and the mixing of several chemicals. During this research many factors on EWOD system design were considered, along with their effect on reliability. Finally, a proof of concept device is proposed which addresses issues and considerations for practical use, such as loading of a disposable cartridge, ease of control, and test diversity, etc.

CHAPTER 3 – PROPOSED DEVICE DESIGN

3.1. OVERALL DEVICE ORGANIZATION

To be an effective PoC device, it must be portable, reliable, and versatile. The design proposed in this research attempts to be effective in all areas by being battery powered, self-aware, and modular. In general, the reagents and sample are loaded into a disposable EWOD chip. The chip is loaded into the device which contains the electronics necessary to activate the pad array according to the assay being performed. Figure 19 shows an overview of the device design. Main device functions and control is handled by an Atmel ATmega328 microcontroller. The device also contains memory space large enough to store a number of assay protocols such that the user can select the appropriate program for the given chip. The memory allows the user the ability to have multiple assay specific chips on hand increasing the devices capability in the field. The microcontroller displays a menu of all assay protocols loaded onto the device. Once a particular protocol has been selected by the user, the microcontroller fetches the first sequence of the protocol from the EEPROM and transfers it to the HV507 high voltage drivers which activate the appropriate pads. The microcontroller then waits for the appropriate voltage to be reached by the droplet position feedback system before fetching the next sequence from memory. This process is repeated until the entire protocol has been processed.

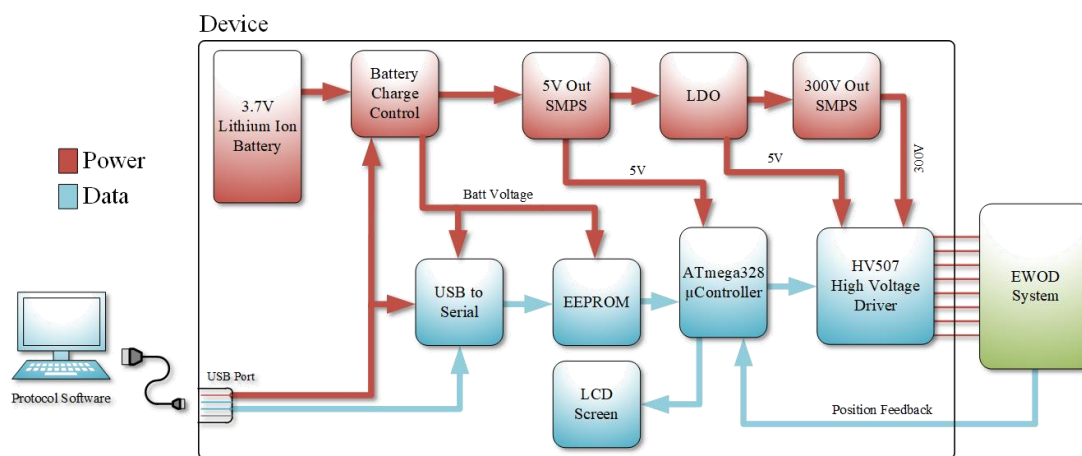


Figure 19 - System block diagram

The programs stored in memory can be managed through custom software on a PC and downloaded to the device via a USB port. Another microcontroller is incorporated to translate the USB packets and store them into the EEPROM. Additionally, a power supply capable of voltage outputs up to 300V is incorporated to offer possibilities

to move many liquid types. Finally, to maximize portability, the entire system is powered from an integrated lithium ion battery which provides hours of testing time. The battery can be recharged via a USB port making for many charging options.

3.2. BATTERY AND POWER DISTRIBUTION

As seen in Figure 19, the power distribution part of the system consists of a battery charge unit, a 5V switch mode power supply (SMPS), low drop out voltage regulator (LDO), and a high voltage SMPS capable of 300V output. The battery charge control unit provides a method of correctly recharging the lithium ion battery when connected to a USB port using the appropriate Constant Current (CC), Constant Voltage (CV) protocol. The 5V SMPS unit ensures that as the battery voltage level drops, as the battery drains, the logic components still receive the appropriate 5V level. The LDO unit serves as a method to reduce switching noise of the 5V supply feeding the high voltage SMPS. Finally, the high voltage SMPS provides the high voltage output for the activation voltage.

To increase portability, the device is designed to operate from battery power. Power consumption must remain low to maximize operating time and make the device practical for many applications. Due to some components already being selected as being an ideal solution for their task, such as the high voltage driver, some parameters such as supply voltage and power consumption have already been determined. The combination of the SMPS, HV507PG, and EWOD system have been routinely characterized during operation of many types of experiments in this research. When configured to provide its maximum activation voltage, the SMPS draws about 300mA of current to the high voltage output. The current draw from the SMPS is highly dependent on the activation voltage, number of pads activated, activation frequency, and size of a pads. As described previously, the SMPS can adjust the output voltage given a constant input voltage. Because the digital control circuits of the HV507PG require 5V to operate, it is logical to use the same voltage rail to provide a 5V input supply to the SMPS. Additionally, the AREF voltage given to the ADC of the microcontroller can only be as high as V_{dd} of the microcontroller. Therefore, to ensure that the ADC has the highest range possible, the 5V rail will also supply the microcontroller and AREF voltages.

A challenge with battery voltages is that the voltage is not constant during operation. As the battery supplies current to the system, the voltage continues to drop. However, a simple solution to this is to incorporate another boost converter SMPS to ensure the battery voltage is always increased to 5V. Other components that do not have specific voltage or performance requirements, such as the EEPROM, were selected based on power consumption and price.

Due to the various supply voltages, care must be given to the fact that logic voltages may be different from component to component. Components which are running at a lower voltages need to be able to withstand logic levels above their V_{dd} coming from components supplied by a higher voltage. Another way to address this issue is to incorporate a level shifter on the appropriate signals. Different logic levels exist between the microcontrollers and the EEPROM. Both microcontrollers will operate at 5V, however, the EEPROM operates at battery voltage (3.0V-3.7V). Conveniently, the EEPROM can withstand logic levels up to 6V, and logic coming from the EEPROM should always be high enough to trigger the logic threshold as needed.

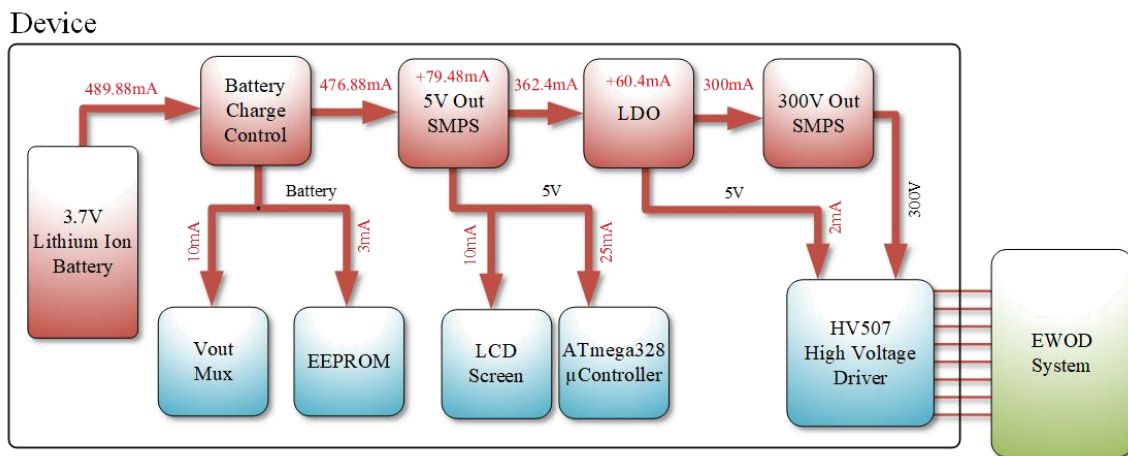


Figure 20 - Estimated current demands through device

It is common for the basic boost converter circuit to produce switching noise on its output voltage since the output voltage node is connected directly to the switching components (diode and MOSFET). The noise is slightly suppressed by the output capacitor, but it is far from an ideal solution. A relatively easy way to reduce the noise on such a signal, is to put a Low Drop Out (LDO) voltage regulator at the output of the SMPS. Voltage regulators designed to produce a clean output voltage from a varying input. The LDO regulators are designed to have input voltages very near their input voltage, which increase their efficiency and limit their power loss. This makes LDOs ideal for power supply noise suppression in portable devices. Regulators were purposely left off of the microcontrollers as they have their own regulators on chip. Adding another regulator in series would only add unnecessary power loss.

Figure 20 shows the estimated flow of current through the device based on component current draw from Table 2. It can be seen that the total current draw seen at the battery is nearly 0.5A. Therefore, a 2Ah lithium ion battery was selected to maximize operating time. All current ratings were assumed to be worst case scenarios, running

at maximum activation voltage and shifting data between the EEPROM and high voltage driver. With a 2Ah battery, the device could run for at least 4 hours. Contributing most to the current demands is the high voltage SMPS driving the EWOD system. As the activation voltage is increased, the current draw increases proportionally. Therefore, running at a lower activation voltage will increase battery life.

Component	Efficiency (%)	Supply Voltage (V)	Current Draw (mA)	Running Total (mA)
300V SMPS		5	300	300
HV Driver Logic		5	2	302
5V LDO HV Driver Logic	80		60.4	362.4
Microcontroller		5	25	387.4
OLED Screen		5	10	397.4
Battery V to 5V SMPS	80		79.48	476.88
Vout Mux		3.7	10	486.88
EEPROM		3.7	3	489.88

Table 2 - List of components current requirements

For instance, many of the liquids moved in this research could be done at an activation voltage under 100V, which would lower the current draw by 200mA. With only a total current demand of ~300mA, battery life could last over 6 hours. It is worth noting that these times represent active testing time, and during any inactive time the microcontroller can disable the high voltage SMPS, significantly reducing current draw. The battery is integrated into the device, therefore charging is done through the USB port. The task of directing available power to and from the battery is done by the MCP73831T by Microchip, which is a lithium ion charging integrated circuit (IC). The MCP73831T charges the lithium ion battery following the CC-CV protocol typical of lithium ion batteries. The CC-CV protocol dictates that the battery is charged by providing it with a constant current until a, specific, fully charged voltage level has been reached. Once the fully charge voltage level has been reached, the voltage on the battery is maintained. In the case of the battery selected for this device, the fully charged battery level is 4.2V, and must be maintained within +/- 0.05V. Battery discharge and charging currents are referred to in terms of “C”, where 1C is equal to the battery capacity. For instance, in the case of the lithium cell chosen for this design, 1C would equal a current of 2A. Typical charging currents for lithium batteries is ½C, and many “fast charging” circuits push the charging current near 1C or more. The risk with any fast charging method is the heat generated in the battery while charging. These challenges have been addressed in today’s electronics by adding battery temperature monitoring and other protections to their circuits. However, to keep charging simple, the charging system designed for this device

would charge at 500mA, or $\frac{1}{4}C$. While this is a much lower charge rate than what is typical, it was selected as a safe starting point for this new design.

There are two Switch Mode Power Supplies (SMPS) used in the device. One to ensure the battery voltage maintains 5V to the other components as the battery drains. The other SMPS is used to increase the 5V supply to the 300V maximum output to initiate droplet movement in the EWOD system. To ensure a large range of activation voltages, in order to accommodate a variety of liquids, a goal of 300V output was set. A switch mode power supply (SMPS), boost converter topology, was selected due to its efficiency and capability to produce a large difference in voltage. The theory behind any SMPS is that a switch is used to convert between two or more different circuits. When combined, they can produce desirable characteristics, such as increasing or decreasing voltage. Figure 21a shows the schematic of a basic boost converter which is a topology of a SMPS DC-DC converter. When the switch is closed, current flows from the voltage source, through the inductor to ground. Current through an inductor is governed by Equation 5 where V_L is the voltage drop across the inductor, and L is the size of the inductor.

$$\frac{di}{dt} = \frac{V_L}{L} \quad (5)$$

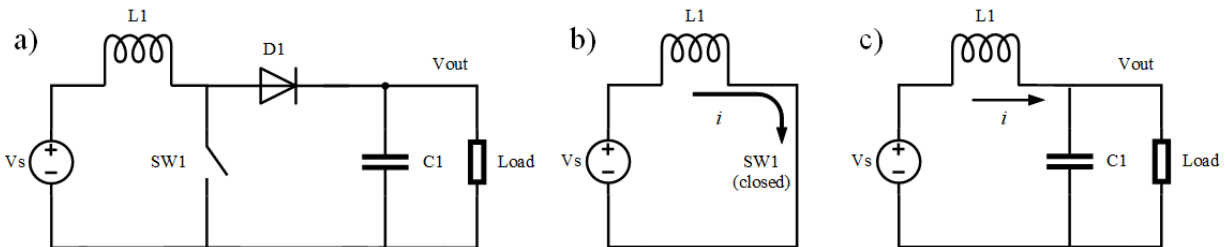


Figure 21 - The basic boost converter schematic (a), circuit when switch is closed (b), circuit when switch is open

In the case of Figure 21b, when the switch is closed, the voltage drop across the inductor becomes the value of the voltage source. As suggested by Equation 5 as long as there is a voltage drop across the inductor, there will be an increase in current (di/dt) through the inductor. If the switch is then opened, the current built up from the previous configuration is diverted to the circuit formed in Figure 21c. As long as the current through the inductor is higher than the current required by the load, charge will build up on $C1$, increasing the voltage output following Equation 6. The switch in Figure 21 is realized as a metal-oxide semiconductor field-effect transistor (MOSFET) where a low voltage digital signal can control its state. When the gate of the MOSFET is grounded (low), the MOSFET is non-conducting,

and the switch open. If the gate of the MOSFET is V_{dd} (high), then the MOSFET is conducting and the switch is closed. Relating the control signal back to the state of the circuit, it can be seen that a *high* signal creates the circuit in Figure 21b, and a *low* signal creates the circuit in Figure 21c. By treating the control signal as a square wave, each state forms one whole cycle of the control signal. The amount of time in each state is then represented by the duty cycle of the signal.

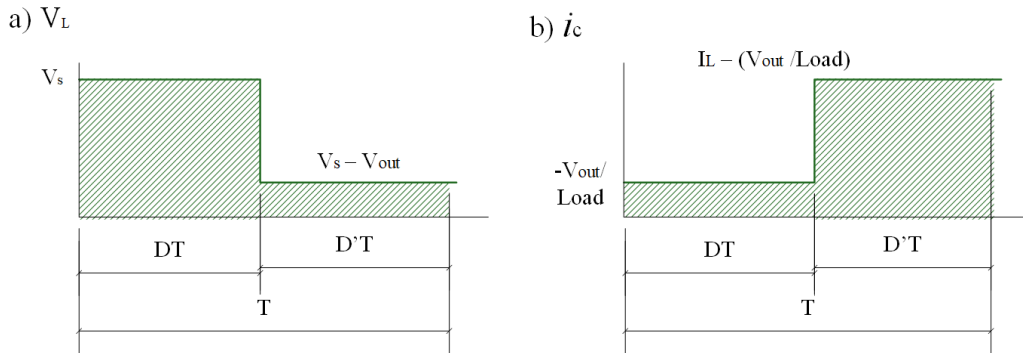


Figure 22 - Voltage and current for each state of the control signal waveform

Figure 22a shows the voltage across the inductor (V_L) for each state of the control signal. Figure 22b shows the current through the capacitor (i_c) of $C1$. In both cases the period of the control signal is represented by the variable T . D is the portion of the duty cycle where the signal is high, and D' is the portion of the period the signal is low. It should be noted that $D' = 1 - D$. As mentioned, as long as there is a voltage drop across the inductor, there will be an increase in current through the inductor. The total magnitude of the current can now be found by referencing the voltage drop across the inductor, and multiplying it by the time spent in that state. Figure 22a shows while the control signal is in the *high / on* state (D), the voltage drop across the inductor is the voltage source (V_s). Multiplying the voltage drop by the fraction of time spent in that state (D), the total charge supplied by the inductor can be represented. Similarly, when the control signal is in the *low / off* state. The same can be done for observing the current through the capacitor $C1$ (Figure 22b). It should be observed that these are simply integrals, or the area under the curve. The switching between two different circuit configurations allows for a charging and discharging of $C1$, which does create a ripple of the output current. However, it is assumed that when the SMPS is operating at a steady the charge and discharge are equal, such there is no net gain or loss in charge. Using this assumption, we can create equations for both V_L and i_c as shown in Equation 6 and Equation 7.

$$V_s D + (V_s - V_{out}) D' = 0 \quad (6)$$

$$-\frac{V_{out}}{Load} D + \left(I_L - \frac{V_{out}}{Load} \right) D' = 0 \quad (7)$$

By simplifying both Equation 6 and 7, an equation for the steady state current (I) and V_{out} can be found (Equation 8 and 9)

$$I_L = \frac{V_s}{Load D'^2} \quad (8)$$

$$V_{out} = \frac{V_s}{D'} \quad (9)$$

It is worth noting that V_{out} is a function of switching duty cycle, as seen in Equation 8. Based in this, the magnitude of the high voltage output can be controlled by the switching characteristics. Additionally, it is governed by the input voltage (V_s). While equations can direct design making decisions, they are based on perfect conditions, so there needs to be considerations given for real world effects. For instance, if one were to plot Equation 9, as seen in Figure 23, they might suspect that any level of output is obtainable should the boost converter apply the appropriate duty cycle.

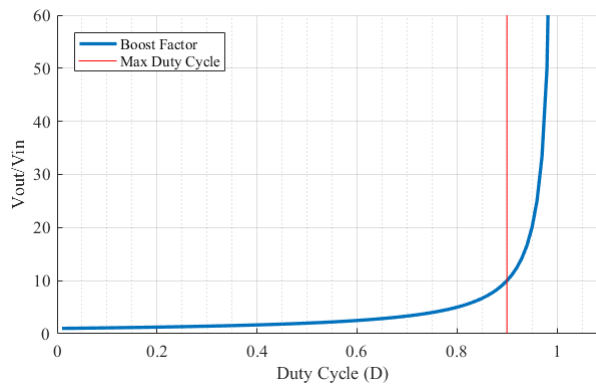


Figure 23 - Boost factor as a function of Duty Cycle

Most boost controlling circuits limit their duty cycle to ~90%. Of course, it also makes sense that a duty cycle of 1 is impossible as no current would have a chance to be delivered to the output sine the circuit would never leave the closed switch state (Figure 21b). Therefore, there exists a limit as to the maximum output voltage obtained by a

boost converter system. If the maximum duty cycle is typically 90%, then theoretically the maximum output voltage will be somewhere around 10x the input (~50V). This thesis challenges these limitations by trying to produce an output range from 60V-300V from a 5V supply.

Due to their switching nature, boost converters also come with a side effect of a fluctuating output current. Considering each state of Figure 22, the magnitude of the current ripple (Δi) can be found. The current ripple is defined as being symmetrical about the steady state current, with Δi above the steady state current and Δi below. When observing the current through the inductor during the *on* state of the control signal (D), the ripple current will start at $1\Delta i$ below steady state and increase to $1\Delta i$ above steady state. Therefore, the peak to peak measurement is $2\Delta i$.

$$\frac{di}{dt} = \frac{v(t)}{L} = \frac{V_s}{L}DT \rightarrow 2\Delta i = \frac{V_s}{L}DT = \Delta i = \frac{V_s}{2L}DT \quad (10)$$

There becomes an inherent challenge when designing a boost controller, which gets exaggerated in a device being developed in this paper. Current ripple can cause premature component failure and excess waste in power. The obvious solution to reduce current ripple, supported by Equation 10, is to increase L . However, this also reduces how quickly the power supply can change its current supply due to changing demands. In the case of this device, a droplet is transported by sequentially activating pads. The sequential activation creates a situation where the power supply is required to quickly deliver enough current to charge a pad to the activation voltage, then drop the charge on the active pad and quickly charge the next pad. A high current demand in a short amount of time means high di/dt , which suggests to decrease L . SPICE simulations were done to establish inductor and capacitor values that would establish the desired 300V. An inductor and capacitor values of 100uH, 4.7uF respectively were selected. However, the simulations could only be so accurate without knowing more about the control signal triggering the MOSFET. As seen Equations 8 and 9 the performance of the power supply is heavily dependent on the switching duty cycle. Simulations are only as good as the switching waveforms given. To simplify the control of the voltage supply and switching signals, the MAX1771 from Maxim Integrated was selected. The MAX1771 is a boost converter controller where the inductor, MOSFET, and capacitor are external. By sensing the output voltage, the MAX1771 triggers the MOSFET to maintain a desired output voltage. The MAX1771 uses a proprietary switch control signal that could not be simulated in SPICE. A proof of concept of the SMPS was built and tested using the simulated inductor and capacitor values, the MAX1771 was

able to produce the 300V goal. Additionally, it was able to control the switching in such a way that could charge the pads to full activation voltage in a sufficient amount of time for proper droplet movement. Recalling from Figure 5, the pad array is mostly a capacitive load, and that the output voltage is based on the charge built up on C1. The derivation of the boost controller equations assumes a steady state current flowing to the Load component. However, in this case the load is a capacitor, so not much current is lost through the load. Rather, the current from the inductor charges both C1 and the capacitive load of the pad array. The capacitive load is what contributes to the quick charging times of the pad by the power supply, despite the large inductor value.

In many SMPS, the diode (D1) is often a source of power loss and inefficiency. Since there is a constant voltage drop across the diode when it is forward biased, any current flowing through the diode is loss. If the power supply has to provide a significant amount of current, the loss from the diode can be significant. Additionally, diodes have a finite amount of time, called *reverse recovery time*, before they become non-conductive when they are reversed biased. During the reverse recovery time, the voltage across the diode is reversed, yet still conductive. In the case of a boost converter, the MOSFET is connected to ground, and if the diode is still conductive, the high output voltage can cause a significant amount of current to flow to ground. It is often desired to replace D1 with a MOSFET to lower power loss through D1, however the added transistor requires slightly more control logic. With the EWOD system being mostly capacitive, the only current the power supply has to provide is enough to charge a pad to the activation voltage. While the current demand is increased if the activation signal is AC, it is still much lower than many conventional applications requiring a steady DC current. Due to the relatively low current demands, and the simplicity of the circuit, the diode was used. When component selections were being made, attention was given to the reverse recovery time of the diode used in an effort to reduce power loss as much as possible.

The boost controller is a clever way to increase the voltage from one supply to another, but it comes with side effects the designer needs to be aware of. In particular, Electro-Magnetic Interference (EMI) and switching noise on the output. The output of a boost controller is particularly prone to switching noise due to the, essentially, direct connection to the MOSFET. Noise seen at the input side of the boost controller is suppressed due to the inductor between the input and MOSFET which, by nature, attempts to maintain a steady current. Noise on the output voltage can be minimized through increasing the output capacitor (C1), but that can affect system performance, and increasing component size is less desirable for small portable devices. The physical size of C1 is already quite large due to the

high voltage values it is designed to withstand. There are other ways to reduce switching noise of the output, but of course, there is always the question of if further suppression is required. Since this boost controller was only supplying the high voltage, and the output voltage was fairly smooth, it was decided to remove the LDO from the system and reduce loss.

Boost controllers are used often in cell phones, laptops, and automotive applications. Many embedded options exist that incorporate the inductor, MOSFET, diode, and capacitor in one small package. However, when dealing with voltages as high 300V, typical components would not support this high of voltage. When the switch is in the open position, *CI* and *DI* would be exposed to the high voltage, so components capable of handling such voltages would need to be selected. The output voltage is sensed by the MAX1771 (net HV_FB in Figure 24) using voltage division from the output. The controller switches the MOSFET (T3) so that the output voltage is high enough to generate 1.5V at the HV_FB node. Voltage division is a simple way to get a fraction of a voltage source based on the ratio of two series resistors as shown in Figure 24

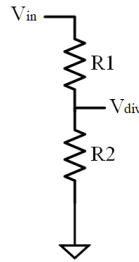


Figure 24 - Voltage division circuit

The voltage seen at V_{div} in Figure 24 can be adjusted based on the ratio of $R1$ and $R2$ following Equation 11. To minimize the power lost through this circuit, large resistance values need to be selected. An arbitrary $2M\Omega$ resistor was selected for $R1$, and $R2$ was calculated given $V_{div} = 1.5V$.

$$V_{div} = V_{in} \left(\frac{R2}{R1 + R2} \right) \quad (11)$$

The device needs the capability to move a variety of liquids which may require different voltages. To reduce the amount of power consumed to as low as possible, a programmable output voltage was incorporated by making the voltage division of the feedback network adjustable. An analog multiplexer was used to select between 8 different

resistors to provide 8 different feedback circuits, and therefore, 8 different output voltages. Table 3 shows the calculated resistance values of the feedback network for the desired output voltage, and the resistor values selected.

V_{sel}	V_{out}	$R_{calc} (\Omega)$	$R_{select} (\Omega)$
0	300	76	50
1	250	2098	2100
2	200	5139	5100
3	150	10228	10200
4	125	14317	14300
5	100	20483	20400
6	80	28243	28200
7	60	41308	41300

Table 3 - Feedback resistor values

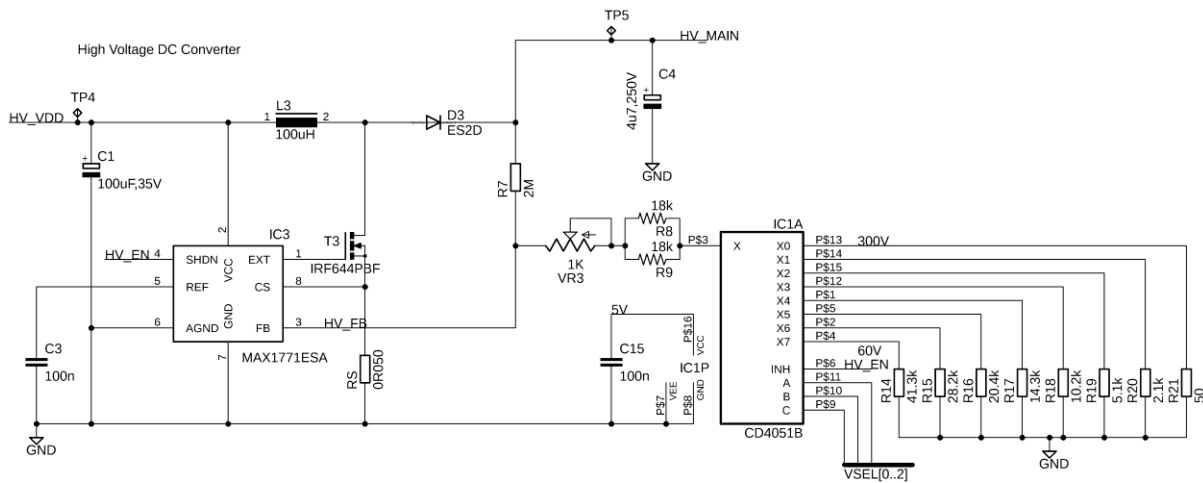


Figure 25 - Complete high voltage DC-DC boost converter circuit

The feedback network in Figure 25 is the combination of resistors $R7$, $R8$, $R9$, $R14-21$, $VR3$ and the analog multiplexer, CD4051B. Resistor array $R14-21$ are the selected feedback resistors from Table 1, and $VR3$ is a trim resistor for voltage output calibration. The appropriate settings will be selected via the VSEL signals from a microcontroller discussed later.

3.3. HIGH VOLTAGE DRIVER

To move a droplet from one pad to another, the pads must be activated sequentially. The process of activation means delivering enough current to the desired pad so that the capacitive pad reaches the activation voltage. In other words, the pad needs to be connected to the high voltage power supply output. Once the droplet has moved fully over the active pad, the charge on the active pad needs to be removed (pad connected to ground). This process is repeated for the next pad in sequence. A simple solution to this is a switch, with a pull-up resistor, connecting the pad to high voltage source as depicted in Figure 26. When the control signal is *low*, the transistor is non-conductive and stops the flow of current through the transistor. The voltage on the pad (V_{pad}) is then charged to HV source. When the control signal is *high* the transistor is conductive, connecting the load to ground.

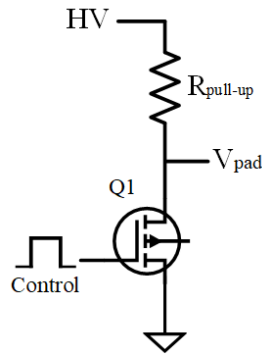


Figure 26 - High voltage driver using pull-up resistor

There are two major disadvantages to this topology. The first is the relatively slow charging of the load to the high voltage source. A long charge time limits how high of a frequency can be used for the activation signal, and in extreme cases, limits the minimum activation time between pads. When the transistor is *off*, it is essentially removed from the circuit, leaving just $R_{pull-up}$ and the capacitive load in series. Charging of the capacitive load, therefore, is limited by the RC time constant (τ) following Equation 12.

$$V_{pad} = HV \left(1 - e^{-\frac{t}{\tau}} \right) \quad (12)$$

To charge the pad quickly, $R_{pull-up}$ must be small, however when the transistor is on, a voltage division circuit (Figure 24) is formed between $R_{pull-up}$ and the internal resistance of the transistor. The intent is that V_{pad} is ground, however, this assumes a large value for $R_{pull-up}$ such that most of the voltage drop from the HV source is across R_{pull-}

up. If $R_{pull-up}$ is low enough the voltage division may cause the voltage seen at V_{pad} to be much higher than ground causing the circuit to be ineffective. The second disadvantage of the topology in Figure 26 is large power consumption. As mentioned, when the transistor is in the *on* state, it forms a voltage division circuit which creates a path to ground. The power lost through this path can be limited by increasing the resistance, however, this increases issues described previously. Since a pad array inherently means multiple pads to control, it means multiple channels losing power. Exaggerating the power loss is the way the EWOD system fundamentally operates. As mentioned, the power loss is only when the pad voltage (V_{pad}) is selected to be ground. However, in typical EWOD operation the majority of the pads are ground with only a select few pads being activated for droplet movement. The total power loss can be quantified by Equation 13, where n_{off} is the number of pads in the ground state (off) and R_{on} is the internal resistance of the transistor.

$$P_{pull-up} = n_{off} \left(\frac{HV^2}{R_{pull-up} + R_{on}} \right) \quad (13)$$

As the assay complexity and number of reagents used increases, the number of pads also increase. Increasing assay complexity therefore increases power loss, which is not conducive to a battery powered device.

The process of charging and discharging capacitive loads is the basis for much of digital circuits, and the Complimentary Metal-Oxide Semiconductor (CMOS) topology is well suited for this task.

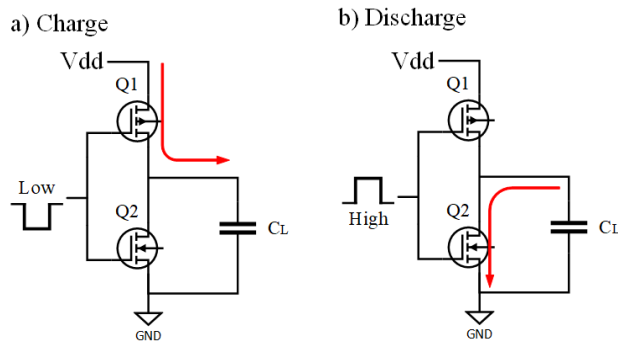


Figure 27 - CMOS topology

The *complimentary* description of the CMOS name comes from the complimentary operation of the output based on the input signals. When connecting the gates of each transistor together, each transistor also operates

complimentary to the other. When configured as in Figure 27, the circuit can be used to charge and discharge a capacitive load (C_L). When a *high* signal is applied to each gate, the NMOS becomes conductive and the PMOS is non-conductive, creating a path to ground which will discharge the load. Similarly, when the gate signal is *low*, the NMOS is non-conductive and the PMOS becomes conductive connecting the load to the high voltage source (Vdd). By applying the circuit to each pad in the array, any pad can be charged and discharged accordingly. More importantly, the charging and discharging of the circuit is done quickly. Each stage (charge and discharge) form a circuit in which there is a resistor and capacitor in series, as in the pull-up resistor topology. However, instead of the large resistive value of $R_{\text{pull-up}}$, only the internal resistance of the transistor is seen, greatly reducing τ . Additionally, the CMOS topology does not continually form a path to ground as in the pull-up topology. However, there is a direct path to ground as the circuit states transition from charge to discharge. Care must be taken during the circuit design to reduce the amount of time spent in this transition period, but the specifics on how to do so are beyond the scope of this paper. Assuming the time spent in the transition period is low, the power consumed by the EWOD system can be generalized by Equation 14.

$$P_{\text{cmos}} = n_{\text{on}}(fCHV^2) \quad (14)$$

Where n_{on} is the number of pads being activated, C is the capacitive load of the active pads, and f is the frequency of the activation signal. The power consumption equations (13 and 14) show the significant differences between the two topologies. In particular, the n_{on} and n_{off} variables. The number of pads active (n_{on}) is typically one, leaving the rest of the pads in the array grounded (off). Since the majority of the pads are grounded, n_{off} can be a large number contributing to a large power loss. However, not only is Equation 14 applied to the pads that are on, but it is also a function of frequency. Combined, it means that the CMOS topology draws much less power because it doesn't continually drain current to ground, and it acts on a much smaller number of pads.

A complication of the CMOS topology in high voltage circuits is the extra circuitry needed to turn off the PMOS transistor. In typical digital circuits, the magnitude of the *high* control signal is the same as Vdd, which is how the signal is able to turn off the PMOS (Q1). However, when trying to drive high voltage circuits, the control signal is typical digital voltages (3.3V-5V). With the source of Q1 being the high voltage source, the gate of Q1 is driven by low voltage circuits, then the control signal would never be high enough to shut off Q1. When driving high voltage

circuits with a CMOS topology a level shifter must be used. Figure 28 shows the same CMOS circuit in Figure 27, but incorporates a level shifter made from a comparator circuit. A comparator circuit uses an op-amp's ability to quickly saturate its output to the rail voltage. The positive input of the op-amp is used as a reference voltage, and the negative input is the control signal. If the control signal is greater than the reference voltage, then the op-amp's output will saturate to the positive rail voltage. If the control signal is less than the reference voltage, the op-amp will saturate to the negative rail voltage. A common configuration for the comparator circuit is to connect the negative rail voltage and positive input (reference) to ground. If the signal connected to the negative input raises above ground, then the op-amp output saturates to the positive supply voltage. If the positive supply of the op-amp is connected to the high voltage source (HV), then the comparator circuit will saturate to the high voltage supply. Figure 28 shows hypothetical voltages being applied to the circuit, and how this translates to voltage on the load. A low voltage control signal is connected to the negative input of the op-amp and the gate of the Q2 (V_{NG}). A *low* voltage control signal (0V) would make Q2 non-conductive just as described in Figure 27. The 0V control signal causes the output of the comparator to saturate to ground, driving the gate of Q1 to ground, making Q1 conductive, and charging the load (C_L). When the control signal is *high* (5V), the gate voltage of Q2 (V_{NG}) is driven high enough to make it conductive. The 5V on the negative input of the op-amp causes the output of the comparator to saturate to the HV supply (300V), which drives the gate voltage high enough to make Q1 non-conductive. The configuration in Figure 28 creates a circuit which can drive high voltages given low voltage control signals.

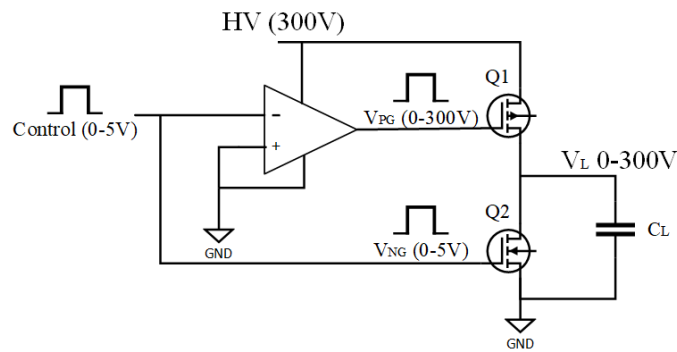


Figure 28 - CMOS circuit driven by a level shifter

Conveniently, there are a few components that offer high voltage drivers in relatively small packages. The Microchip Technology HV5XX series of chips, which are serial to parallel converters with different number of output channels, and capable of handling a variety of high voltages. As the name suggests, serial to parallel converters accept

serial data in and delivers the data in parallel form. As shown in Figure 29, serial data is clocked into a shift register. Each clock pulse reads in the next serial bit, and shifts data that has already been read. After data has been shifted into the register, a pulse on the latch signal latches each bit into a flip-flop and presented to the output in parallel. The signals from the parallel output are used to drive the control signals of the high voltage driver circuit in Figure 28. The serial to parallel converter and CMOS high voltage driver together create a system capable of driving a high number of EWOD pads.

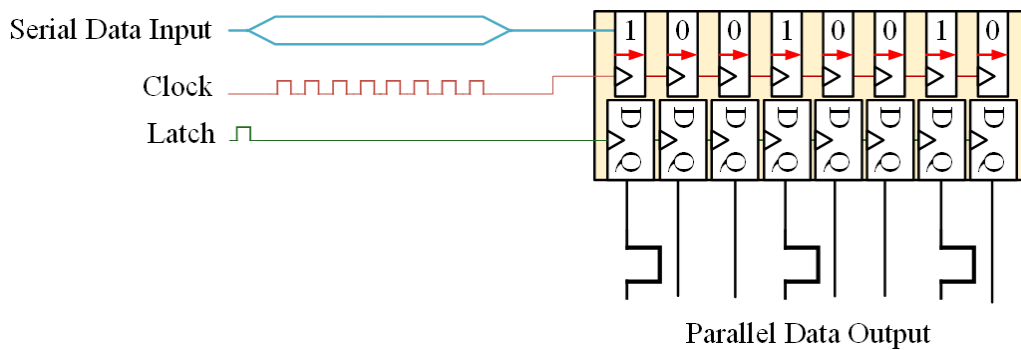


Figure 29 - Diagram of serial to parallel converter

The Microchip Technology HV507PG is a serial to parallel converter with 64 channels that can drive up to 300V to its outputs. It uses a serial communication protocol described in Figure 29, where serial data is clocked in and latched using three different signals. The proposed device is capable of driving up to 128 pads, therefore, two HV507PG components are used in series to produce the 128 high voltage outputs.

3.4. ON BOARD MEMORY

Since the device needs to drive up to 128 different pads, any combination of active pads depends on a 128-bit binary number. Since droplet movement depends on the sequential activation of pads, a new 128-bit number must be shifted into the two drivers. Each 128-bit number corresponds to the active pads in the EWOD array pattern. To activate a pad in the first sequence, a specific 128-bit combination represents that pattern. To activate the next pad, a new 128-bit pattern is sent. This process is repeated as many times as needed to complete an assay. The 128-bit combinations for each sequence are stored in order in a EEPROM Memory. A EEPROM memory is a memory structure where the contents of the memory can be changed at any time. It is also non-volatile, meaning the contents of the memory will not be erased when power to The non-volatile the memory is lost. feature is ideal for battery

powered devices because the data will not be lost should the battery die or need replacing. It also makes device design easier as the device can simply be switched off by disconnecting the power to all components. No backup power is needed to maintain the memory contents.

Most memory structures are made up of a multiple spaces to store data, otherwise known as *words*. Each word is given an address so that it can be accessed individually. The size of each word varies, but is often 8 bits, and there can be a wide number of words in one structure. Figure 30 gives an example of a typical memory structure with 4096 8-bit words. With the high number of words, it is conventional to represent the address in hexadecimal since a binary representation would be too long (12 bits in this case). The total size of the memory is calculated by multiplying the word size by the number of words. In the example given in Figure 30, it is 8 bits by 4096 producing a 32,768 bit memory, or simply 4096 kilobytes (kB). To store data that is larger than the width of the word, it will then require multiple addresses to be used. For instance, to store the 128-bit number for the high output driver in the example memory structure in Figure 30, 16 words will need to be used. If the 128-bit number was stored starting at address 0x000, then it would take up the next 15 addresses (0x000 – 0x00F). It is up to the system designer to determine if the Most Significant Bit (MSB) of the 128-bit number is stored first or the Least Significant Bit (LSB).

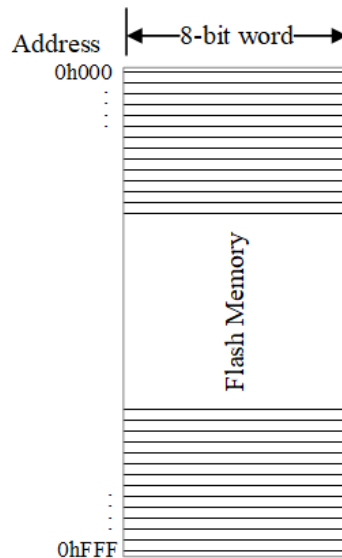


Figure 30 - Memory structure example

The EEPROM selected for this design is the STMicroelectronics M95M02-A125 which is a 2Mbit memory with 8-bit words. Data can be written or read from a given address. To minimize pin count of the memory package,

data is sent in and out of the memory module serially using the Serial Peripheral Interface bus (SPI). Similar to how data is shifted into the high voltage driver, the SPI protocol transfers data bit by bit on every clock pulse. A major difference is the chip select pin which the master controller sets low to enable data transfer to the memory chip. To define where data is written to or read from, instructions are required in a format defined by the memory manufacturer. Data in the SPI protocol is typically broken up into bytes, therefore, the instructions are made up of multiple bytes consisting of address bits then data. When reading data from memory, the initial address that the data is stored in needs to be sent. After a starting address is sent to the memory chip, the controller continues to send a clock signal, and the data at that address is returned. If the controller continues to send a clock signal, the memory chip automatically increments the address, and returns the next byte. By sequentially storing each 128-bit number required to complete an assay into the memory, the assay can be followed by simply incrementing down the memory address space.

3.5. MICROCONTROLLER

For proper movement of droplets, there must be a way to control the sequence of pads and the timing between each activation. There can be many ways to complete this task such as PC or bench top equipment. However, to incorporate this system into a small hand held style device, the control must be done with an integrated circuit. Preferably, a microcontroller as it incorporates several embedded dedicated circuits. Figure 31 is a block diagram of a typical microcontroller. At the heart of all microcontrollers is a microprocessor which is responsible for general computation and program navigation. The unique features of a microcontroller are the integrated peripherals such as Analog to Digital Converter (ADC), timer, serial communication, and General Purpose Input and Output (GPIO). Different manufacturers and models have varying combinations of peripherals, but it is always true that there is more than just a microprocessor. A dedicated program is loaded onto the microcontroller and stored in the integrated memory. The microprocessor executes the instructions of the program which can be simple mathematical operations, or can be access and control of one of the peripherals. For instance, to send data over serial communication, the microprocessor can send data from computations to the dedicated serial communication hardware. Once the microprocessor transfers the data to the serial communication hardware, the microprocessor can continue executing instructions of the program. Meanwhile the dedicated serial communication hardware sends the data according to the configured protocol. The integrated dedicated hardware allows the microprocessor to easily interface other hardware giving a project high functionality. For this research a microcontroller will execute a dedicated program to activate the correct pads at the correct time. Pad activation will be controlled via serial communication to the HV507PG

(driver). Serial communication is done through the dedicated serial communication hardware of the microcontroller utilizing the SPI protocol. The HV507PG uses a serial communication protocol is very similar to SPI, but lacks the Slave Select (SS) signal. The SS signal is used to control which slave device gets the data. With the SS missing from the HV507PG, any data on the SPI bus will be clocked into the shift register of the driver regardless if the data is meant for the driver or not. Incorrect data transfer to the HV507PG is avoided because the microcontroller controls the latch signal of the driver, therefore data will not be presented to the driver output until the latch signal is pulsed. As long as data designated for the driver is the last data on the SPI bus before the latch is triggered, then the driver output should be correct. Conflicts on the SPI bus should be easily avoided since the microcontroller is the sole controller of the bus.

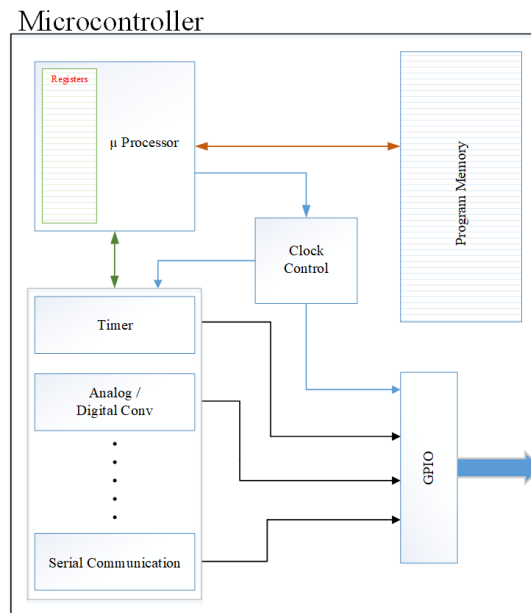


Figure 31 - Microcontroller block diagram

Any additional signals that are not part of a standard protocol, such as the latch signal, are handled using the GPIO peripheral of the microcontroller. The GPIO is a set of low voltage, low current, drivers that can be controlled by the microprocessor embedded in the microcontroller. There are several input / output (I/O) pins grouped into *ports*, and each pin can be programmed to be a dedicated input or output channels. The GPIO contains configuration registers that are used to set up the various pins as needed, and data registers that are used to drive or read the status of a pin. If a pin is set to be an output, storing a 1 or 0 in the appropriate bit of the data register drives the pin to Vdd or ground respectively. Similarly, pins configured as inputs can be sensed high or low by reading if the appropriate data bit is a

1 or 0. Other peripherals of the microcontroller need access to the outside world, such as serial communication and ADC. To save package save and reduce pin count, it is often the case to use the GPIO peripheral as the interface between external connections and other peripherals. For instance, when configuring the serial communication peripheral to specify common parameters such as baud rate, protocol, etc., the GPIO will have to be configured to route specific pins to the serial communication peripheral instead of being controlled by the microprocessor.

Another convenient peripheral is the Timer, which is used when time critical operations are needed. It works by incrementing a counter starting from zero, at a specific rate, to a programmed *match number*. When the counter equals the match number, the timer triggers an event, typically an interrupt. Interrupt Sub-Routines (ISRs) can be thought of as a separate program function that only gets executed when called. In this case, the interrupt is what makes the call, as opposed to a specific call in the main program. The use of the interrupt further increases the timing accuracy because the task that is time critical does not have to wait for any code from main to finish executing. Once an interrupt is received, all other code execution is halted, and the ISR is executed immediately. The Timer and interrupt are used in combination with the GPIO to produce the pulse wave of the activation signal at the correct frequency. The HV507PG driver has an input pin (BL) that will *blank* all of the outputs low when the BL pin is high, no matter what data is currently latched. When the BL pin is returned to ground, the latched data is returned to the outputs. Using the Timer peripheral of the microcontroller, the frequency of the activation pulse wave can therefore be programmed. Based on the desired frequency, the appropriate match value can be calculated and stored in the Timer peripheral. The ISR is programmed to simply toggle a given pin in the GPIO. Together, when the appropriate amount of delay has past, the timer reaches the match number and triggers an interrupt to the ISR. The ISR toggles the GPIO pin which is connected to the BL pin of the driver. By toggling the BL pin, a pulse wave is generated on all active pads.

When the device is first turned on, the micro controller ensures proper startup of the various components used and when ready, ensures the high voltage is at the desired levels. As mentioned previously, the boost converter SMPS uses a MAX1771 controller which uses a voltage division circuit to monitor if the output voltage is correct. It adjusts its switching pattern based on V_{div} (Figure 24) being 1.5V. This means that the output voltage is at desired levels if $V_{div} = 1.5V$. Using the ADC peripheral of the microcontroller, V_{div} can be monitored to determine if the desired voltage levels have been met and allow the assay to start. Additionally, they can be monitored during the assay and halt the progress if the voltage drifts outside of a given range. Voltage monitoring improves the reliability of the

device because voltage levels may drop low enough to reduce DEP forces, or high enough to risk dielectric breakdown. Pausing the assay gives time for the SMPS to regain stability of the output voltage before proceeding producing more consistent performance. The 10-bit ADC peripheral contains dedicated hardware to the analog to digital conversions on a given I/O pin without the use of the microprocessor. The results of the conversion can be retrieved by the microprocessor where further computations can be done. The voltage on the analog input pin is compared to a designated analog reference pin (AREF). The magnitude of AREF is divided into 2^M quantization levels, where M is the number of bits of the ADC. In this case, the microcontroller contains a 10-bit ADC, therefore, the reference voltage is divided into 1024 quantization levels. An analog input voltage of 0V (ground) would return 0, and a voltage equal to AREF returns 1024. Assuming the AREF value is known, the voltage of the analog input by calculating the ratio of the returned digital value (D_{Bin}) and the ADC resolution following Equation 15.

$$V_A = AREF \left(\frac{D_{Bin}}{2^M} \right) \quad (15)$$

The resolution of an ADC is defined by the voltage value of each quantization level, shown in Equation 16.

$$Res = AREF \left(\frac{AREF}{2^M} \right) \quad (16)$$

The main job of the microcontroller in this device is to control the high voltage driver by providing the correct 128-bit pattern to activate the appropriate pads on the EWOD system. Since all of the 128-bit patterns for the entire assay are stored in order in the EEPROM memory, the microcontroller is programmed to simply read the memory and transfer the data to the driver. Once the droplet has moved to the active pad, the next pattern is read from memory and transferred to the high voltage driver. The microcontroller repeats this process until all of the patterns have been sent.

3.6. EWOD SYSTEM DESIGN

For a sample preparation system to be successful in a PoC device, it must be able to perform a variety of tasks so that it can support many different assays. It must also be extremely reliable such that it avoids breakdown and consistently moves liquids as desired. To evaluate the performance and practicality of the system, the Nucleotide Removal Kit by Qiagen was performed on the device as well as a custom bead binding protocol. The process for extracting Nucleic Acids (NA) such as DNA is fairly complex for an automated system. Figure 1 shows the basic

DNA isolation protocol used by many NA isolation kits. First, the sample must be mixed with a lysing buffer to break open cells in the sample and release the DNA. Next, the DNA is forced through a provided filter using a centrifuge. The DNA binds to the filter, but is mixed with unwanted material such as cell wall fragments, proteins, etc. A wash buffer is then run through the filter to wash away any unwanted material, leaving only the DNA bound to the filter. To release the DNA from the filter, an elution buffer is used to break the bond between the DNA and filter. The result is a solution containing only DNA from the given sample. To implement such a large protocol, a more diverse chip was designed for the EWOD system. Figure 32 shows the pattern selected for the pad array which could implement the entire Nucleic Acid (NA) extraction protocol.

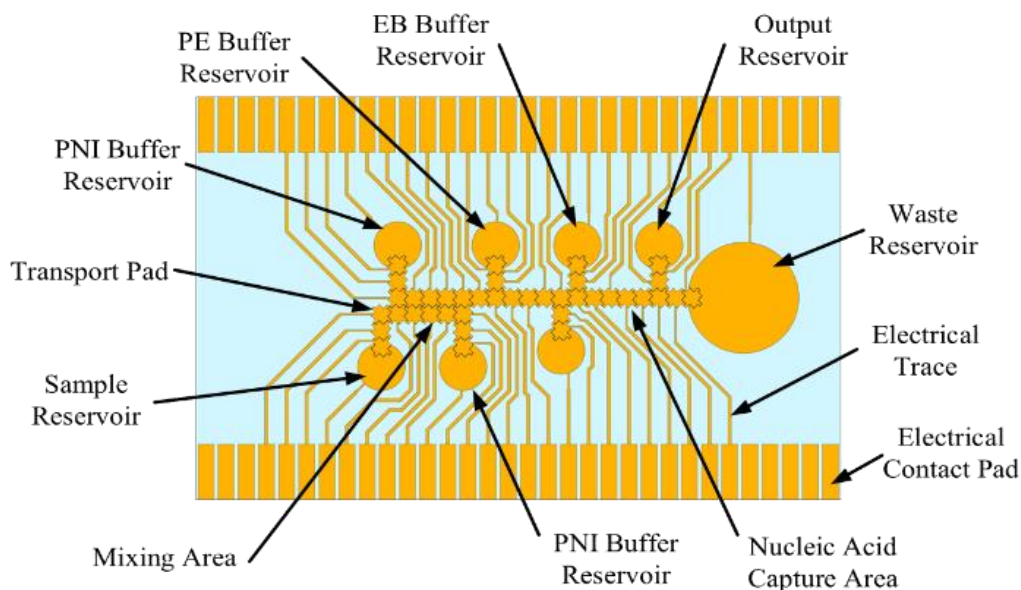


Figure 32 – Nucleic Acid extraction chip design

There are 49 pads in total including the reservoir pads. There is one reservoir for a sample input, one to hold waste liquids, and one output reservoir. There are five other reservoirs for kit reagents and a group of 10 pads creates an area for liquids to be mixed. The overall process for many NA extraction kits are relatively similar to the processes described in Figure 1, therefore, this pattern will accommodate a variety of DNA extraction kits. The lab based DNA extraction kits expect a certain ratio of reagents be mixed for the kits to be effective. Therefore, the ratios were kept the same despite using significantly smaller volume of sample and reagent. The EWOD conveniently makes ratio mixtures easy since the size of the transport pad dictate the volume moved. The size of the pads are the same, so the ratios are controlled by simply moving the correct quantity of droplets into the mixture. The transport pad size was

arbitrarily chosen to be 1mm square. A saw tooth edge design was used to help increase the chances of movement from one pad to another, as discussed previously. Ultimately a ground plane height of 260 μ m was used, although, experiments show the device operated correctly at 130 μ m. A higher ground plane height was found to ease the process of loading liquids. To maintain the correct height of the top plate, and to contain the desired media, two layers of 3M 468MP (130 μ m thick) double sided tape was laser cut to form a perimeter around the pad array. To be monitor movement performance, the ground plane was constructed of glass with an Indium Tin Oxide (ITO) coating so that the plate remained transparent. Holes were drilled to provide loading ports to the reservoirs. The top plate was placed on top of the double sided tape, securing it to the pad array. The EWOD electrode pattern was constructed on a 1"x3" microscope slide using a metal evaporation method which allowed our lab to keep the manufacturing process in house, and reduce turnaround times. To perform the photolithography process, masks were designed in AutoCAD and manufactured by CAD/Art Services (Bend, OR). A layer of Rohm Haas S1813 photoresist was applied to a glass slide using a spin coater for 5s at 700 rpm, then 30s at 3000 rpm. The masked photoresist was exposed to UV light for 10s. The slides were then developed for 2min and plasma cleaned for 2min right before evaporation. A 20nm layer of chromium was evaporated to the slide, followed by a 130nm layer of gold.

3.7. POSITION FEEDBACK

To be a robust and reliable system, the device must be able to detect and account for situations that do not end up in complete droplet movement. Common situations being dirt in the EWOD system, manufacturing variations resulting in surface imperfections, dielectric breakdown during operation. Therefore, the device must be able to detect if the droplet has successfully reached its destination, and for this, a position feedback circuit method needs to be incorporated. Various designs based on impedance [41] or capacitive sensing [42], and image sensing [40][30] have been developed to monitor droplet position and movement. Image based systems are often used in research to validate EWOD performance, and could potentially find their way into Lab on Chip (LoC) devices as image sensors get smaller and less expensive. However, image based systems require supporting systems that make them less than ideal for droplet sensing. The first is simply that the image sensor needs to "see" the droplet. This is not an issue for most labs doing research on EWOD because the top plate is usually ITO coated glass, which remains transparent. The ITO application is a relatively expensive process and would not be desirable in practical applications. The image processing required to detect a droplet would so intensive would also make the system more complicated and less efficient than

other designs. The ability to detect the droplet during the different stages of movement is not trivial. For instance, the image system must be able to distinguish between the droplet tail, unintended split, or an incomplete transfer.

Many of the impedance and capacitive sensing techniques use a method where the impedance or capacitance of the previously active pad is compared to the currently active pad. The theoretical benefit of this method is that measurements become relative. It is assumed that before the droplet moves, the impedance or capacitance is measured across the starting pad location. This sets a target value for the impedance or capacitance for the destination pad, which removes the need for specific information about the material that may change absolute values. However, demonstrations of these methods fail to account for geometric differences between pads. They also assume ideal conditions, and as this research will reveal, manufacturing variations affect circuit equivalence no matter how they are measured. Another downside of these methods is the added complexity of the system. Since the measurements are relative between two pads, switching mechanisms must be incorporated to sense any two pads of the array. Additionally, measurements must be taken in between activation pulses so high voltage does not affect measurements or its circuitry. Therefore, additional timing and sequencing methods need to be implemented. This research develops a simple and practical system, where concerns of other research are minimized through total system design.

It has been discussed that the active pad in the EWOD system and droplet form an equivalent electrical circuit (Figure 5). Additionally, it was noted how the circuit changes as the droplet overlaps more of the active pad. The position feedback circuit takes advantage of these changes to determine droplet position. Figure 33 shows the position feedback equivalent circuit developed by s. Shih et al [43], which is a simplified version of Figure 5. What may not be obvious at first, is that the circuit is a simple voltage division circuit formed between the EWOD system and measurement circuit. Since the droplet is a conductive material, and the media is a dielectric, the resistance across the EWOD system changes dramatically if the droplet is above the active pad or not.

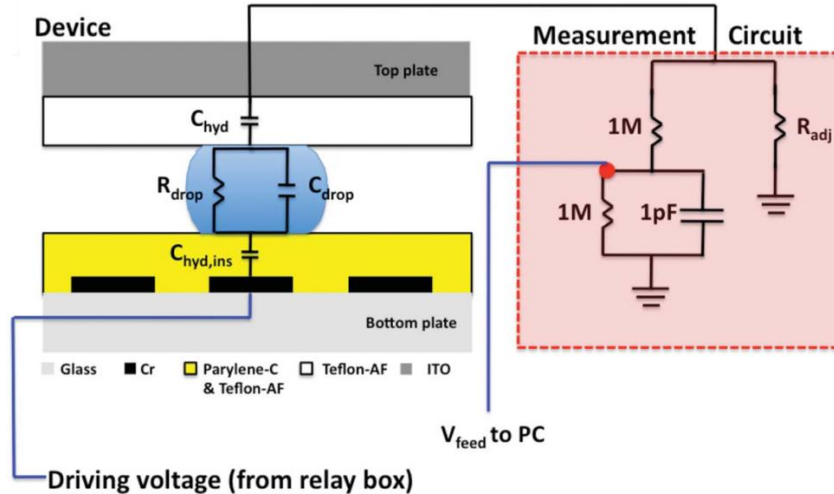


Figure 33 - Position feedback equivalent circuit

When the pad is first activated, and the droplet has yet to move, the resistance of the material is extremely high due to the media being a dielectric. As described in Figure 5, the equivalent circuit before the droplet moves over the active pad is a capacitor. Voltage division in this scenario causes most of the voltage drop to be across the dielectric media. The circuit in Figure 33 can be related to Equation 11 by substituting the equivalent impedance of the EWOD system with R_1 , and the equivalent impedance of the measurement circuit with R_2 . The high value of R_1 causes V_{div} , in this case V_{feed} , to be a small fraction of the active pad voltage. For instance, the resistance of R_1 is so high, that the value of V_{feed} is nearly 0V. However, once the droplet moves completely over the active pad, the dielectric media is displaced and the value of R_1 is much lower. The voltage on V_{feed} is still much lower than the activation voltage, but it can be tuned by adjusting the value of R_1 . Using magnitude of V_{feed} as a position sensor may imply that the circuit in Figure 33 produces a DC voltage at V_{feed} . However, as discussed previously, the activation waveform is a pulse wave which would also produce an AC signal at V_{feed} . Given that the dielectric material forms a capacitor (Figure 5), the DC component of the pulse wave is removed making the signal seen at V_{feed} that same as the activation signal, but symmetrical about 0V. To make V_{feed} easier to sense using the ADC of the microcontroller, it is desired to make the feedback signal closer to a DC signal. Therefore, the circuit was reconfigured to contain a half wave rectifier. Since the signal at V_{feed} has no DC component, only half of the waveform is greater than 0V, making a half wave rectifier well suited for converting the square wave amplitude to a DC signal. Figure 34 shows the same voltage division circuit shown in Figure 33, made up of R_1 and R_2 with the half wave rectifier added. When V_{FB} is above V_{Don} , the diode becomes forward biased allowing a portion of the current from the voltage division circuit to charge Cr. When V_{FB}

falls below V_{Don} , the diode becomes reversed biased and prevents charge from leaving C_r . The next pulse of V_{FB} charges C_r more which increases the voltage over C_r .

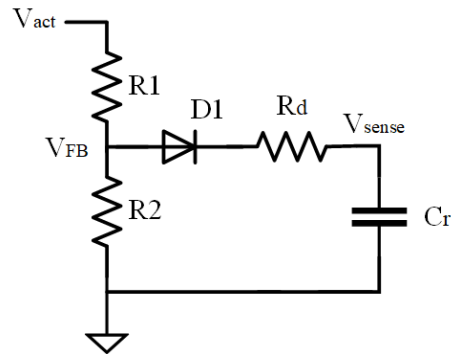


Figure 34 – Position feedback with half wave rectifier circuit

Another way to view the operation of the circuit is the diode produces a pulse wave based on the square wave from V_{FB} . The capacitor (C_r) and resistor (R_d) produce a low pass filter with an RC constant (τ) of $C_r R_d$ which smooths the signal closer to DC. Again, the ADC peripheral of the microcontroller can be used to monitor the voltage of V_{FB_DC} allowing the program to be more intelligent and responsive to actual conditions.

Consideration must be given to the magnitude of the threshold voltage as it impacts the performance of the position feedback network. To maximize the information obtained from the position feedback network, it is preferred to use a threshold voltage that is near the analog reference voltage. Using as much of the analog range as possible reduces the number of bits lost to noise. When obtaining the results for Figure 46, a fixed voltage of 5V was supplied to AREF of the microcontroller. Using a lower reference voltage only increases the percentage of the noise floor to the available range, commonly referred to as Signal to Noise Ratio (SNR). SNR can be calculated using **Error! Reference source not found.**, and given 0.12V of noise (V_{noise}) with a dynamic range of 5V, the SNR is calculated to be 32.4dB.

$$SNR_{dB} = 20 \log_{10} \left(\frac{AREF}{V_{noise}} \right) \quad (17)$$

The ability for the device to change activation voltage increases its functionality, but also increases position feedback complexity. As discussed, the voltage sensed at V_{sense} is a function of the activation voltage and $R2$ of the

voltage division network. Increasing or decreasing the activation voltage linearly affects V_{sense} accordingly. Small fluctuations in activation voltage are not an issue, however, the device can be programmed to provide a wide range of activation voltages from 60V-300V, resulting in large variation of noise magnitude. Lowering the activation voltage lowers the magnitude of the noise seen at V_{sense} thanks to voltage division of the feedback network, however, it also lowers the maximum value obtainable by V_{sense} . If a fixed reference voltage is used, then lowering the maximum value of V_{sense} lowers the effective range of the ADC. For instance, if the ADC uses a reference voltage (AREF) of 5V, but V_{sense} can only produce a maximum of 2.5V, half of the ADC resolution is not being used.

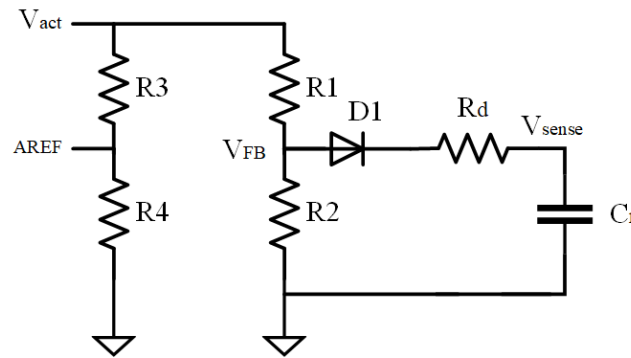


Figure 35 - ADC voltage reference (AREF) obtained by voltage division

Since the noise on the V_{sense} is proportional to the activation voltage, and SNR is the ratio of noise to ADC range, a voltage division circuit can be used to make AREF dynamic. Figure 35 shows a voltage division circuit to obtain AREF, which makes AREF a function of the activation voltage (V_{act}). Using voltage division to obtain AREF has the advantages of being very simplistic and the ability to automatically compensate for fluctuations on V_{act} . Because AREF, V_{sense} , and its noise are all fixed ratios of V_{act} , the SNR is fixed. However, as described previously, voltage division circuits offer another path to ground which contributes to power loss. An alternative is a fixed AREF value that can be obtained through power channels already available, such as the microcontroller Vdd. It is worth noting that V_{sense} is a function of V_{act} since is still based on a voltage division circuit. Therefore, lower values of V_{act} will result in lower values of V_{sense} . the magnitude of V_{sense} is lower for lower V_{act} values, closer examination reveals an increase in SNR. Because the ADC has a finite resolution (Equation 16), lowering the magnitude of the noise seen on V_{sense} lowers the amount of resolution lost to noise. It should be recognized that the resolution of the signal is also lowered, but not a significant amount to affect the operation of the position feedback network. Figure 36 shows a comparison of SNR of the position feedback network when a fixed AREF value is uses versus a voltage division

circuit. Because the SNR increases for lower voltages, and does not lose additional power through a voltage division circuit, the fixed AREF method was selected for the device design.

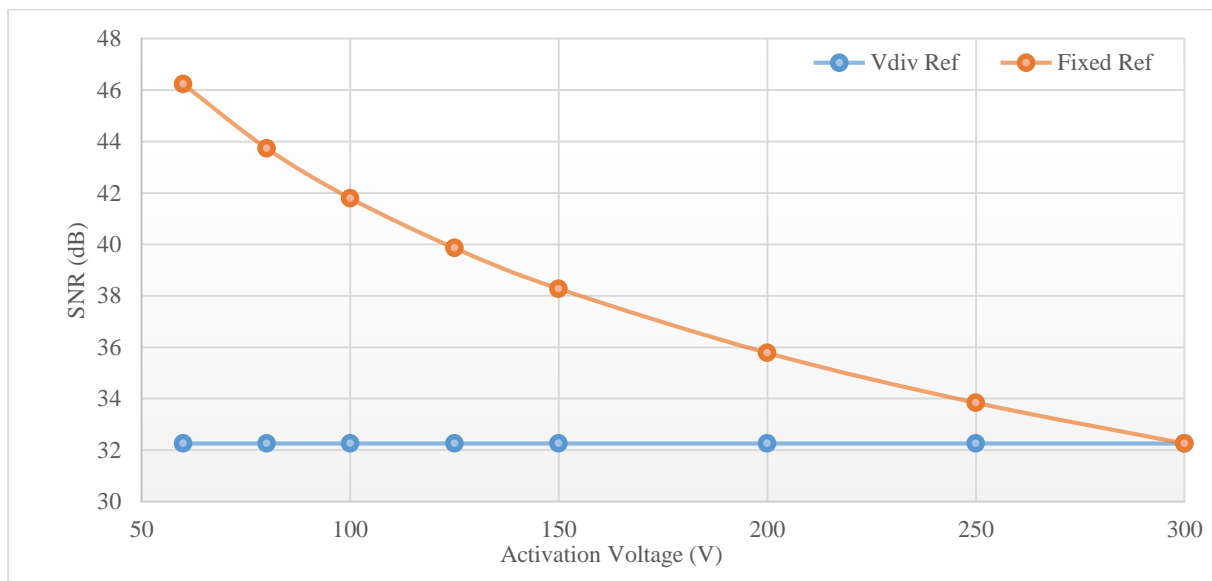


Figure 36 - SNR for fixed reference voltage and through voltage division

The incorporation of the feedback network was another significant step in increasing the EWOD system reliability. If the designated threshold voltage has not been reached, then activation continues. Areas of the EWOD device that contain damage, that slow droplet movement, are recognized by the device which will wait for complete droplet transport before continuing.

3.8. USER AND DEVICE INTERFACE

It would be ideal if the device could be used by a person with limited knowledge of sample preparation, which means it must be easy to use, yet versatile to accommodate a variety of sample preparation protocols. To lay a foundation to accommodate these goals, a crude user interface was developed to load the device with the data needed to prepare samples, as well as interact with the device during operation. The device was made to be portable, however, the information that tells the device how to prepare the sample must first be loaded into the on-board memory. In general, the user will connect the device into a PC loaded with custom software that knows how to communicate with the on-board memory. Files on the PC contain the sequence of pads to be executed in order to prepare the sample, where one file is dedicated to that protocol. The user, via the custom software, selects the files (protocols) to be

conducted off-line and downloads them to the device. Once transfer of data is complete, the device is ready to be used in the field where the user selects the protocol to be executed via a OLED screen and keypad.

The method for populating the on-board EEPROM memory with the desired set of 128-bit patterns is with the use of another microcontroller dedicated to the task. The USB to serial microcontroller is only powered by the USB port, not only to save power, but remove the large programming overhead required for USB communication from the main microcontroller. An Atmel ATmega16U2 was selected for the task of translating USB packets into serial data since it is currently used for a similar task on many Arduino boards. The microcontroller is loaded with a dedicated program that receives USB formatted data and sends it over the SPI bus, specifically, to the EEPROM memory. The microcontroller is seen as a virtual com port to the PC making software development relatively easy and convenient. The virtual com port supporting libraries are standard in current Windows operating systems, which allows software to be written without the need for custom libraries or special installation procedures. The PC software is designed to load a file containing the sequence of patterns to be executed by the device. Since the on board EEPROM memory is more than sufficient to store elaborate tests sequences, multiple tests can be stored and recalled once the device is disconnected from the PC. Because the main microcontroller only has 32kBytes of program memory, the methods required to navigate loaded programs, monitor droplet movement, etc. must be kept to a minimum. For this reason, most of the system validation must come from the PC software before data is loaded into memory. Any validation or information that can be obtained during EEPROM loading should be done ahead of time. Appendix A shows the way data will be stored on the EEPROM. General system information is placed at the starting address (0x000). The first byte contains the quantity of programs that are currently stored into the EEPROM, since the PC software knows how many programs it will be sending. Additionally, since the loading of data follows a set format, the PC software can also calculate the starting address of each program. With the total number of programs and their starting addresses, the microcontroller no longer needs the code overhead to calculate this on its own. Following the system information is any program information that was loaded. Each program contains all of the information necessary to prepare a sample, including program name, number of sequences, and associated threshold values. Program information is broken up into two sections, Header and Protocol. The header information contains the program name, total number of sequences in the program, and the activation voltage used. The protocol information contains the 128-bit pattern and associated threshold level for that sequence. The maximum number of programs that can be loaded onto the device is dependent on how many sequences are in each program. However, assuming each

program only had one sequence to execute, the device could store 62,060 programs. The 2Mbit memory could also store 1 program containing 113,776 sequences.

As mentioned, the format is meant to reduce the overhead of the firmware needed by the microcontroller. By having the total programs loaded, starting address, program name, etc. available in a predefined format, the microcontroller simply needs to read from memory and direct data to the appropriate location. Appendix B shows the workflow of the firmware loaded onto the microcontroller. Because of the helpful formatting of the EEPROM, the workflow can be kept simple, and program size low.

CHAPTER 4 - SYSTEM IMPLEMENTATION, VALIDATION, AND EXPERIMENTAL RESULTS

4.1. SYSTEM IMPLEMENTATION

For the proposed system to be practical as part of a PoC device, efforts were made to make the entire system as small as possible. However, when generating voltages as high as the ones discussed here, electrical components inherently become large. In particular, the capacitor and inductor of the high voltage SMPS are extremely tall compared to the other components. The first method of dealing with extra height of these components is to arrange their placement in conjunction with the battery. The lithium ion battery used, while only 6mm thick, is relatively large when compared to other components. The placement of the battery and high voltage components are such that the components are allowed to rise up beside the battery, keeping the overall height down to that of the capacitor (Figure 37).

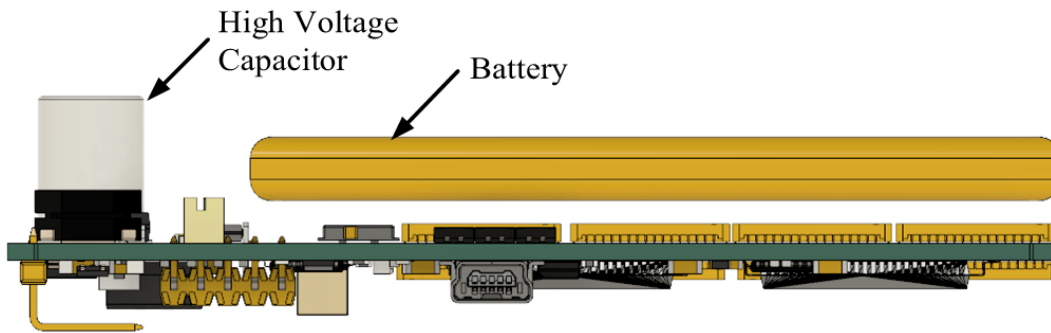


Figure 37 - Side view of PCB and battery showing placement relationship

The size of the battery also dictated rough area restrictions for the rest of the PCB in which all components could be placed. With the components for the high voltage SMPS in place, the rest of the components were grouped by functional blocks, and placed on the remaining PCB area. By placing the battery and PCB together as one unit, the overall dimensions of the main electronics are 99mm x 55mm x 20mm (3.89in x 2.17in x 0.89in), or roughly the area of a cell phone. Placement of functional blocks were based on the flow of power with the goal of keeping the resistance on the power planes low. Figure 38 shows how the different functional blocks are arranged together on the PCB.

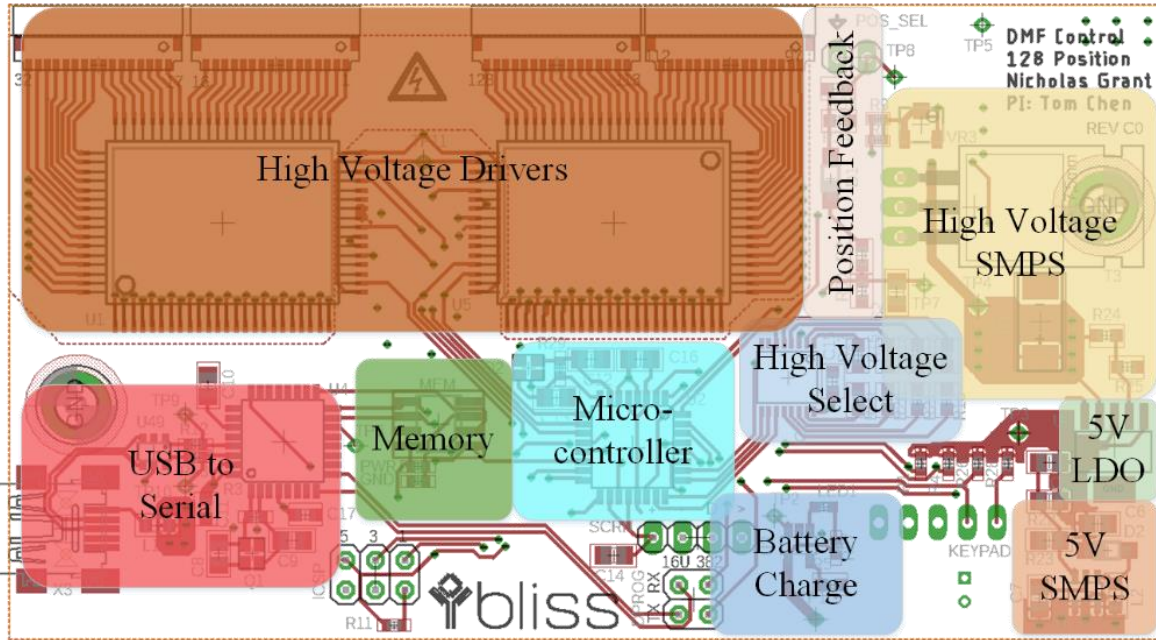


Figure 38 - PCB layout by functional blocks

Appendices A, B show the full device schematic and associated layout. The PCB is a two-layer design where the top layer is the ground plane and bottom layer contains the various power planes. Due to the various supply voltages needed, power planes were broken up accordingly. However, in an effort to reduce Electro Magnetic Interference (EMI), a solid ground plane was used. Most open areas on each layer were filled with ground plane as well to reduce influences from environmental noise, offer additional grounding points, and promote lower noise voltage sources. Steps were taken in the layout design to mitigate potential crosstalk between the high voltage activation signals and surrounding traces. The high voltage signals traveling from the high voltage drivers to the EWOD chip are a unique challenge not typical of most electronic circuits. The pulsed nature of the activation signal, combined with its high voltage is a high risk for coupling surrounding signals. When pulse travels across a digital trace, there is an equivalent pulse following through the ground path. If the signal trace is above a ground plane, the disturbance in the ground plane can be detected in surrounding signals traces. To minimize the disturbance made by the activation signals to surrounding signals, the ground plane was simply removed in the area of the high voltage drivers. Careful placement of the high voltage connectors also ensures that traces on the top and bottom layers are not routed directly above and below each other. Another area of risk, but more common in today's circuits, is the SMPS. As discussed, the output voltage is controlled by the switching of the MOSFET, which introduces switching noise into the supply rail. Careful placement and routing of nonrelated components around the SMPS helps mitigate switching

noise from being coupled onto surrounding signals. Additionally, the components for the two Switch Mode Power Supplies were arranged to reduce induced EMI from high di/dt current loops. Finally, test points and multiple programming ports were also added for debugging purposes.

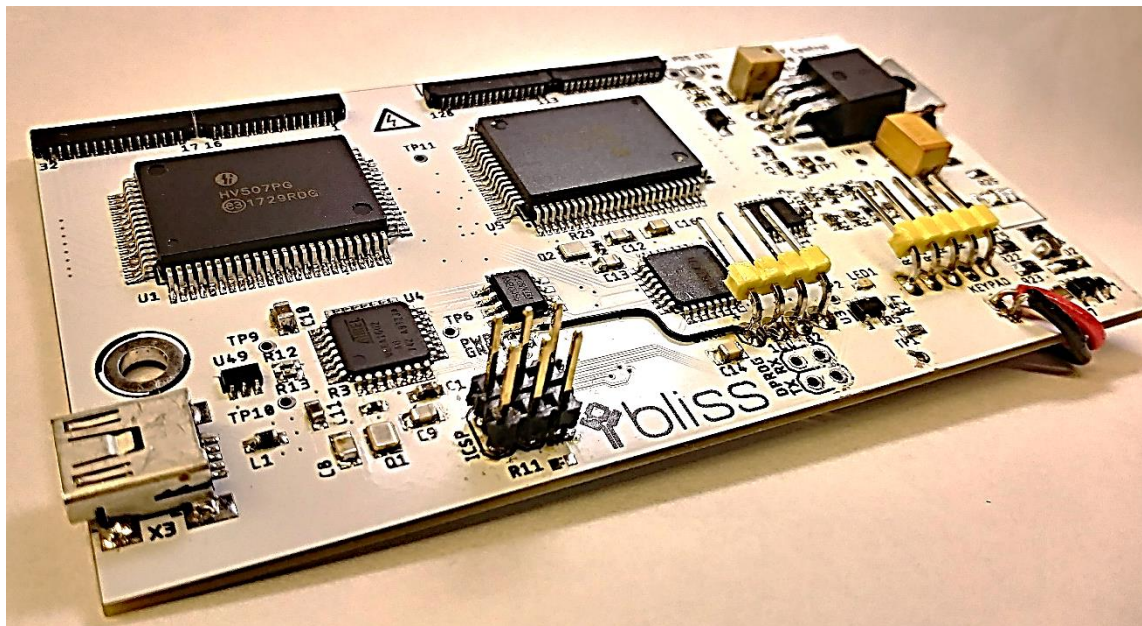


Figure 39 - Finished and populated circuit board

Since the EWOD chips are intended to be used only once, a convenient way to replace the chips for a new test needed to be developed. The interface between the control electronics and EWOD chip presents many challenges. First, is simply the relatively high number of connections to be made. Another is the high voltage the connections must handle, and finally, the small amount of space they are allowed to use. Early EWOD designs, such as shown in Figure 12, had a low number of pads so headers were attached to the chip which could accommodate jumper wires. This method worked well for early demonstrations and testing, however, it was quickly recognized that it was not practical for a larger pad count or for quick and easy chip replacement. The most intriguing option was a card edge connector, which is designed to have PCBs with surface mount contacts on one edge, slide in and out as needed. These types of connectors are used extensively in PCs and servers as memory, video card, and expansion card connectors. The contacts are designed to accommodate cards being inserted and removed repeatedly with minimal damage to the card or connector. However, the traditional card edge designs produced several issues. First, the amount of material that had to be pushed into the card edge connector before it would make contact was around 6mm (0.25”), which meant the majority of the EWOD was covered by the connector, and left little room for sample prep and ground plane.

Another was the majority of the edge connectors available are meant for specific applications, such as DDR memory cards, which meant the connectors conformed to those specific interface standards. For instance, most memory and expansion cards have a slot in the card towards one end for orientation purposes which interfered with our design. Additionally, to accommodate a large number of activation pads and functionality, the pitch of the contact pads on the EWOD chip was reduced to 1.27mm (0.050”), where many card edge connectors were 2.54mm (0.100”) pitch.

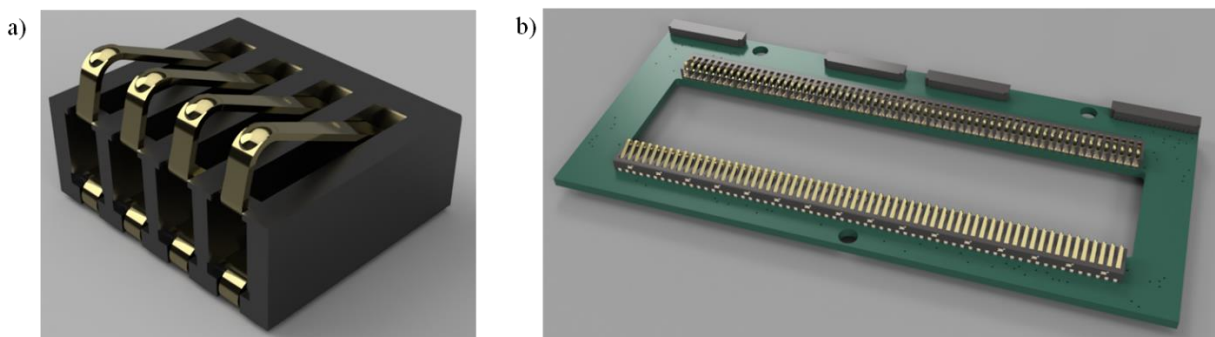


Figure 40 - a) Compression connector b) Complete EWOD chip adapter board with compression connector array

A solution was found by using compression connectors meant for rigid battery pack with integrated electrical contacts. The main use for such connectors and battery packs was the cell phone market before batteries became integrated into the phone. Therefore, these contacts are meant for high use cycles and have a small form factor. The 70ABJ-4-M0E by Bourns was selected due to having the correct pitch and the contact points being near the edge, which reduced the amount of area of the EWOD chip lost to the connector. It was found to make the most efficient use of space on the EWOD chip, contact pads would need to line both sides of the chip. Therefore, multiple 70ABJ connectors were placed side by side on a custom adapter PCB which would transfer the high voltage signals from the cables coming from the control board to the 70ABJ connectors.

Finally, all electronic components were brought together into a custom case, which would not only protect the electronic components, but make it easy to change EWOD chips for new assays. The case holds the LCD screen and keypad, but also a lid that properly locates the connection adapter board around the EWOD chip. The lid snaps closed creating a secure electrical connection to the EWOD chip, and can be quickly released with a push of a button.

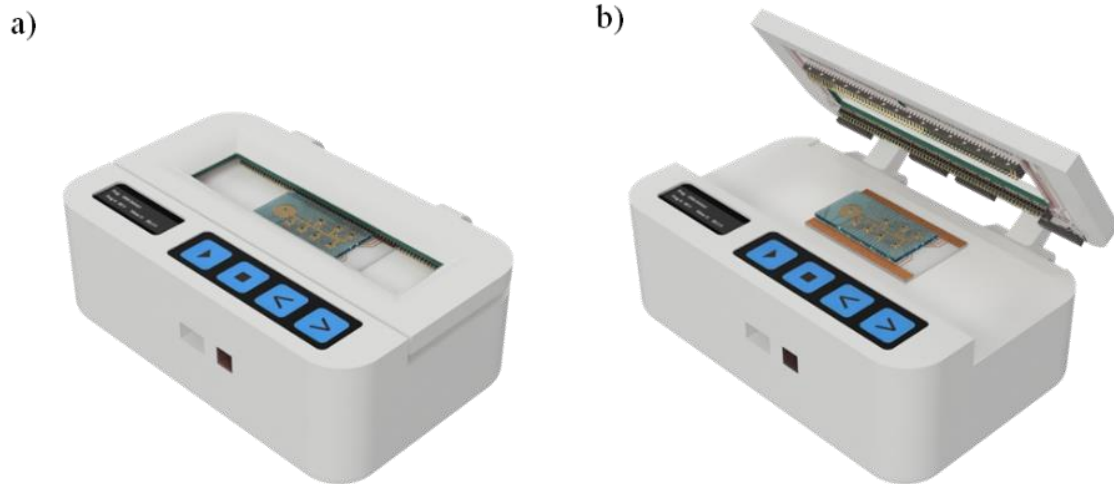


Figure 41 - Complete device showing EWOD chip loaded. a) Closed b) Open

4.2. SYSTEM VALIDATION

4.3. POWER SUPPLY RESULTS

Functionality of each section of the system design was tested as the system was built up, starting with the battery and charging system. First the battery discharge was characterized by discharging it at a constant current of 450mA, which would closely represent the estimated max system current draw. The test was able to more accurately describe the battery's true capacity as well as help establish threshold voltages for the battery level indicator. Figure 42 shows the recorded battery discharge characteristics. The battery is advertised as a 3.7V, 2Ahr lithium ion, where 3.7V is its nominal operating voltage and 2Ahr is its capacity. The recorded initial voltage and discharge curve are typical of lithium ion types where the unloaded, fully charged voltage is near 4.2V for 3.7V cells. Lithium ion batteries also exhibit a sharp drop off in voltage near the end of their capacity, as seen in these results. However, the full capacity fell short of the advertised 2Ahr. With the steady 450mA draw, the battery was only able to stay above the 2.75V cutoff voltage for about 3.125 hours, suggesting a capacity closer to 1.4Ahrs.

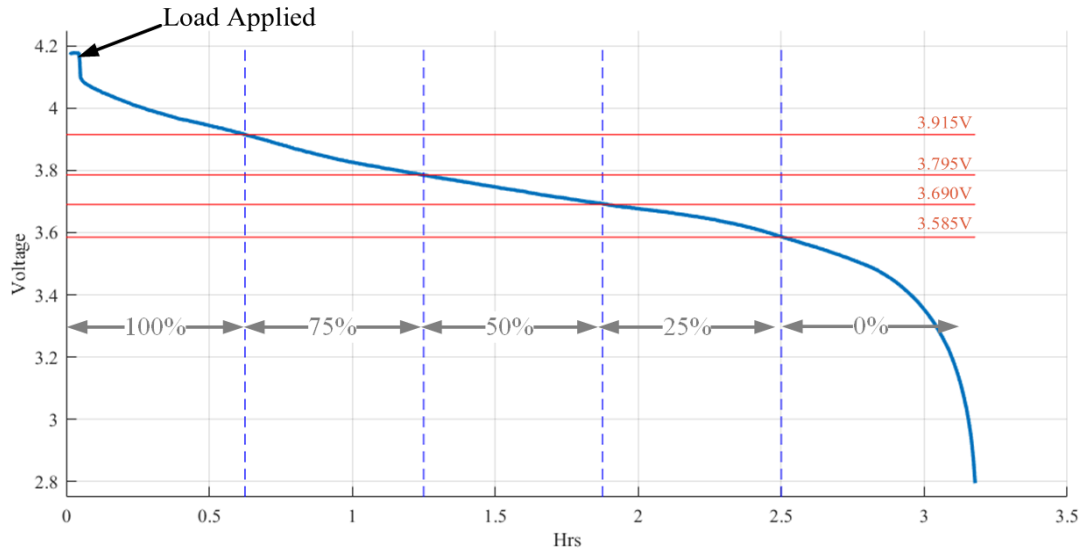


Figure 42 – Lithium ion battery discharge curve

Even with the true capacity of the battery being lower than advertised, with the minimal current draw of the device, it is still capable of operating for several hours at max load. Given that most sample preparation can be done within minutes; practical use of the device would see battery life much higher.

Lithium ion batteries require a specific charging sequence, where a constant current is supplied until a specific battery voltage has been reached, as described in section 3.2. Figure 43 shows the battery voltage while charging. A constant current of 500mA ($\frac{1}{4}$ C) is delivered to the battery until the fully charged voltage of 4.2V is reached. After the fully charged voltage is reached, the charging controller changes to a constant voltage circuit to maintain the 4.2V. During testing of the charge controller, slight overshoot was detected when the max charge voltage was reached, however, it remained just inside of the controller's specifications and within the built-in battery protection circuits. The battery was successfully charged without any detectable increase in temperature.

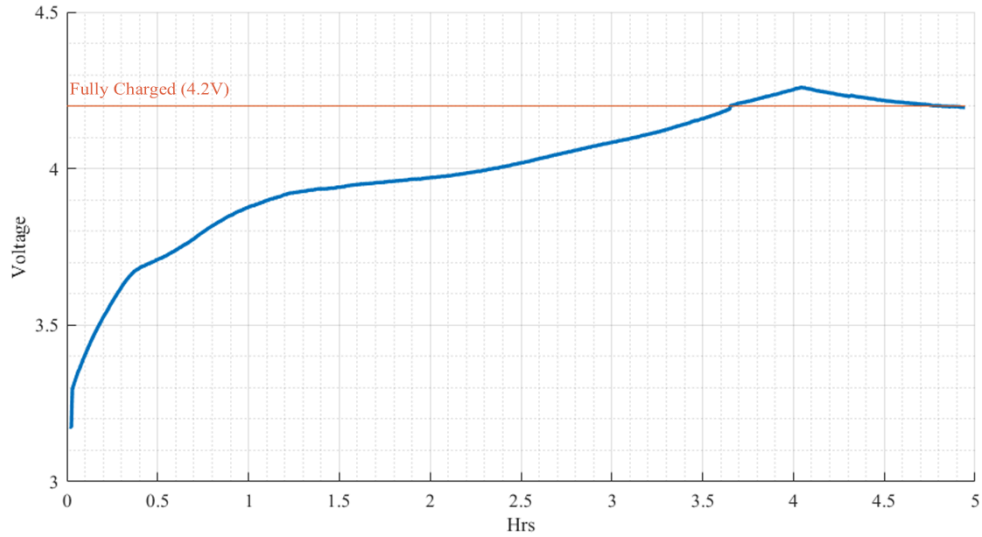


Figure 43 - Charging curve for lithium ion battery

The power from the battery and charging system feed the 5V boost converter responsible for keeping the system voltage at 5V as the battery drains. Both battery voltage and boost converter output voltages were monitored as the system was powered on and off. Figure 44 shows the output voltage of the 5V SMPS as the system is powered on and off. It can be observed that the boost converter quickly reaches the correct output voltage with no overshoot or ringing.

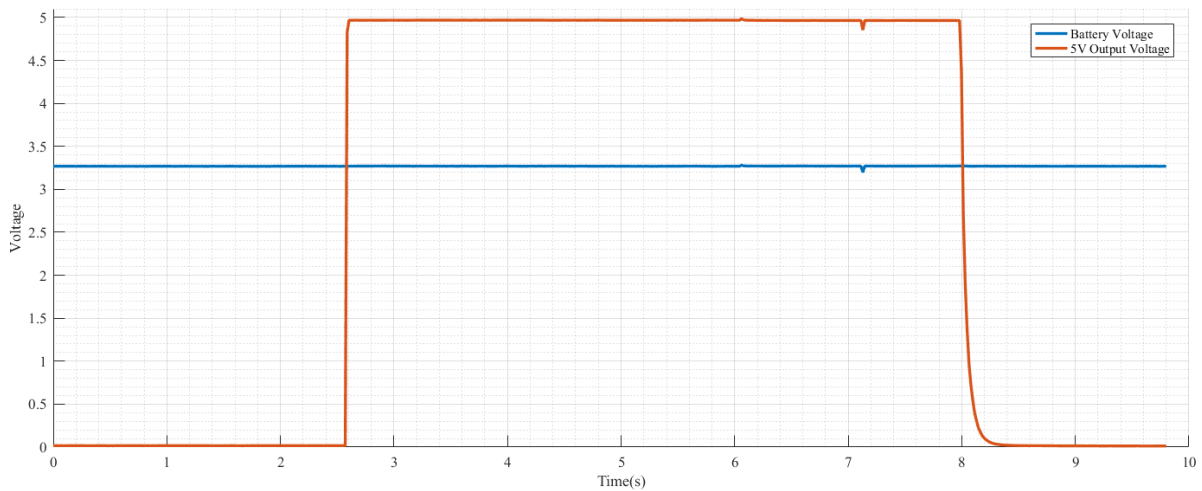
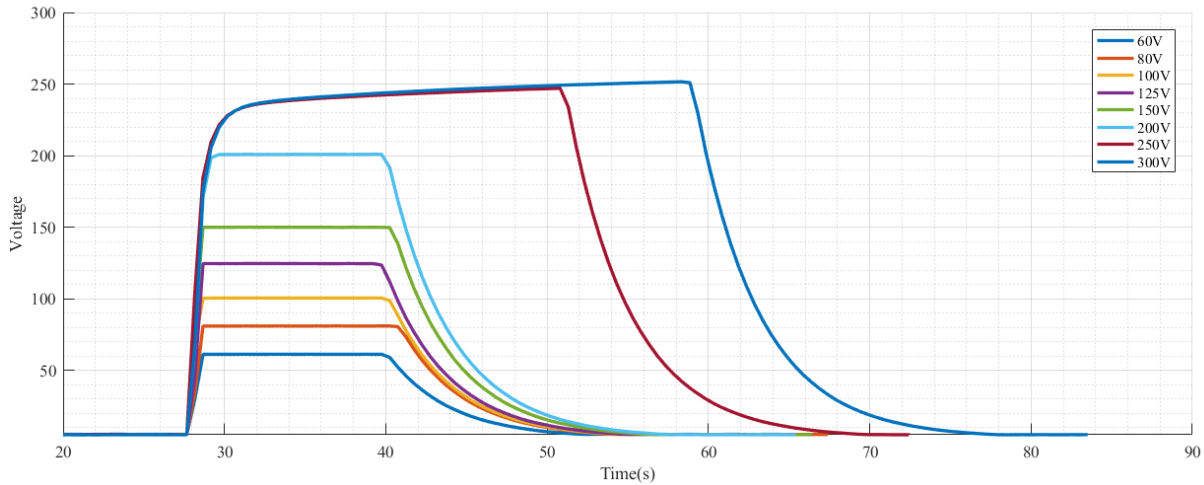


Figure 44 - 5V SMPS output during power on and off

Additionally, when the device is switched off, the voltage quickly drops to zero with minor RC settling time near 0.5V. The high voltage boost converter was also recorded during enabling and disabling of the high voltage circuits.



Along with capturing the rise and settling time of each voltage level, the maximum voltage capability was also observed. All voltage levels up to 200V were reached within 2 seconds, but voltage levels 250V and 300V could not be reached in a reasonable amount of time. As mentioned earlier, obtaining such a large boost factor would be challenging as it would require low parasitic loss and high duty cycles. Obtaining a reliable boost factor near 40x (200V) is very satisfactory. All components were selected to withstand the high voltages as well as estimated currents.

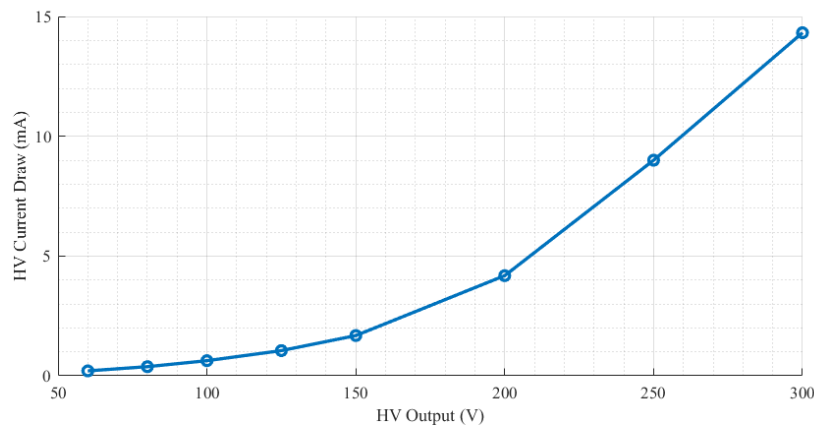


Figure 45 - Current draw from High Voltage circuits

However, the current consumption of the high voltage circuit was measured (Figure 45) to be much less than estimated. During testing of voltage levels 250V and 300V, no increase in component temperature was experienced which is typical of overcurrent or saturated inductors. It is suspected that the MAX1771 controller has simply hit its duty cycle limit and can no longer support these higher boost factors.

4.4. POSITION FEEDBACK RESULTS

The capability of the feedback circuit was demonstrated by recording the values of V_{sense} while a program moved a droplet in a loop over a select group of pads. Figure 46 shows the recorded values of V_{sense} over time by the ADC peripheral of the microcontroller as droplet was cycled around the loop manually four times.

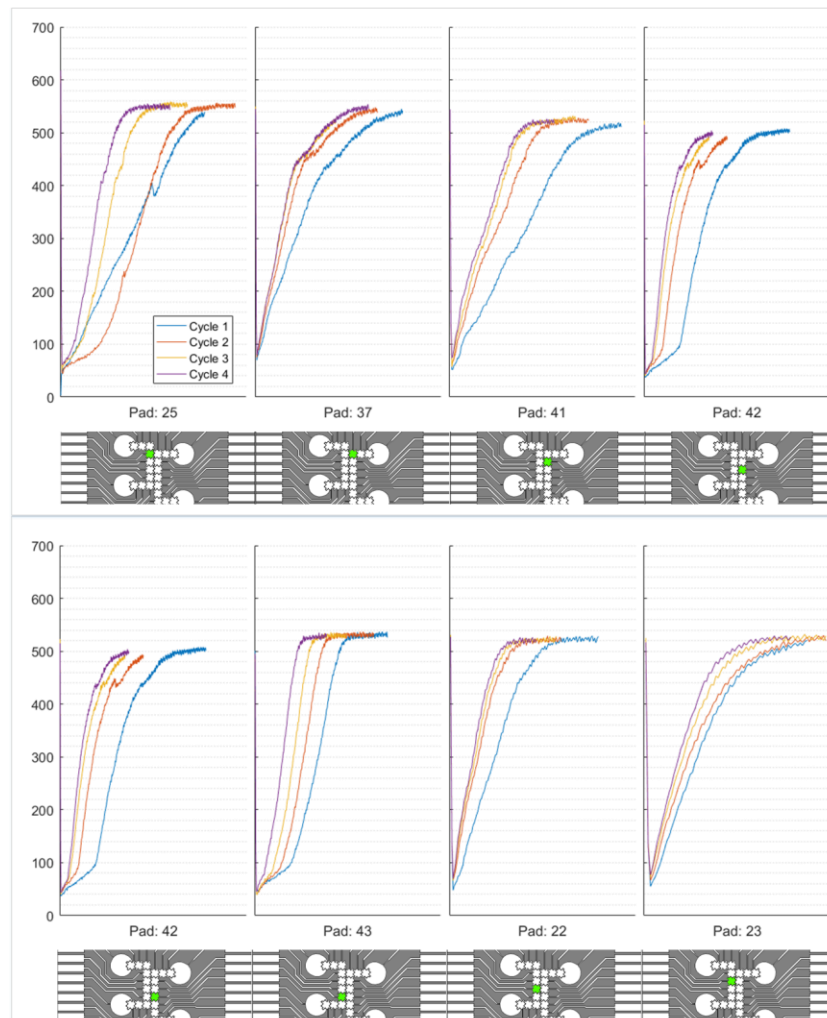


Figure 46 - V_{sense} results for multiple cycles of movement

Most of the pads show ideal results where the magnitude of V_{sense} asymptotes to similar values as the droplet moves over the active pad. In these situations, setting a threshold voltage can trigger the actuation of the next pad in the sequence. Additionally, it can be seen that on each pass of the loop, the same threshold voltage is reached. Pad 24 highlights possible damage to the pad resulting in a slightly higher voltage seen on V_{sense} . Since the majority of the voltage drop from the active pad is over the droplet and dielectric layer to form R1, any damage caused by breakdown lowers the resistance, which raises the voltage over R2. Some pads, such as 43, show a slower rise to its max voltage during the early cycles, and droplet movement becomes faster with every additional cycle. This implies that the droplet is becoming easier to move with each use. Longer movement time is a result of higher resistive forces on that pad possibly due to surface imperfections. Pads 25,37 have slightly higher max voltages which could also be caused by manufacturing variations. These variations are what is considered the limitation of the voltage division method of feedback, and where relative sensing methods are suggested to be superior since individual threshold voltages do not have to be recorded. However, relative sensing methods do not account for these variations either, and are also faced with the same challenges. Developing the device using the EEPROM memory described previously, makes individual threshold voltages relatively easy to implement as the values could be stored with each 128-bit pattern. The main program of the microcontroller is extremely simple and small because it simply increments down the EEPROM memory address. If a droplet transfer is detected to be incomplete, it can simply decrement the address and retry the previous step, possibly with a higher threshold voltage. The small program size also leaves room for more complex algorithms or basic machine learning which could detect errors in movement and adjust accordingly.

It can be seen in Figure 46 that once the droplet has reached the active pad, V_{sense} has minor fluctuations caused by noise from the V_{act} signal. The low pass filter in the feedback network is what smooths the pulse wave from the diode into a DC voltage. Larger R_d and C_r values can further reduce the noise seen on the V_{sense} signal, however, there are diminishing returns. Additionally, increasing component size is a concern for small devices such as being proposed in this research. However, the bigger concern is the conflict between reducing noise and settling time. Once the appropriate threshold voltage has been reached, the next pad in the sequence is activated. At this time the threshold voltage is required to return to zero by removing the charge on C_r . Higher values of R_d reduce noise on the V_{sense} signal, but it also requires more time to drain charge from C_r . Therefore, it can take a measurable amount of time for V_{sense} to return to zero. Indeed this issue can be seen in Figure 46, partially well on pad 23, where the initial samples from the ADC are near the voltage levels from the previously active pad. Because the microcontroller can operate and

sample the V_{sense} signal quickly, the ADC may sense an incorrect value due to the residual voltage. There are multiple ways to reduce the potential for reading an invalid value such as reduce R_d or additional circuitry. As eluded to previously, lowering the value of R_d will only reduce the effectiveness of the low pass filter in the feedback network. Additional circuitry can be incorporated to quickly discharge C_r before activating the next pad, but this adds complexity and size to the overall design. Instead, a simple delay is added to microcontroller program to allow V_{sense} to settle back to zero.

4.5. EXPERIMENTAL RESULTS

4.5.1. DNA ISOLATION

4.5.1.1. IMMOBILIZED FILTER METHOD

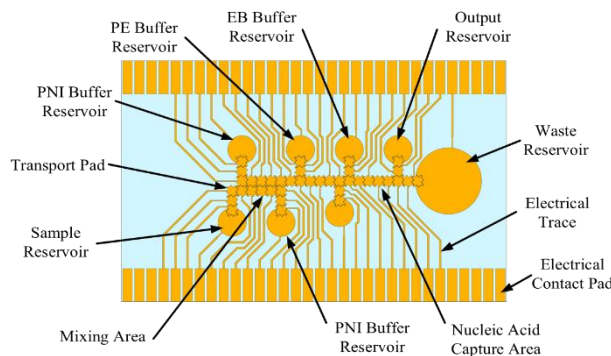


Figure 47 – EWOD design for filter method

To test the design, the Nucleotide Removal Kit by Qiagen and its protocol were replicated on the device. As discussed previously, silicone oil is used as the media to improve EWOD performance and reduce evaporation of the liquids in the device. Figure 47 shows the location of all liquids used in the protocol. The Nucleic Acid Capture Area defines the location of the DNA binding material. To prepare the chip for protocol execution, roughly 50 μ L of 1cSt silicone oil was placed into the EWOD system using a pipette until all air was displaced. A fluorescently tagged DNA with an initial concentration of 1 μ g/ μ L was diluted 10:1 in DI water. Roughly 2 μ L of the dilution was loaded into the sample reservoir. Two other reservoirs were filled with 2 μ L of the PNI buffer supplied with the kit. Another two reagent reservoirs each were filled with 2 μ L of the PE and EB buffers. The PNI and PE buffers were pre-diluted with either ethanol or isopropanol as instructed by the Qiagen instructions. The device was then programmed to pull one volume (260 μ L) of the sample and move it to the mixing area. To maintain the same ratios as instructed by the kit, 5 volumes of the PNI buffer were pulled and moved to the mixing area. The sample and PNI buffer was mixed in the

mixing area by activating the pads in a circular motion. The solution was then moved to the DNA capture area for binding, one volume at a time. Excess volume would pass through to the waste reservoir. Next one volume of the PE buffer would be moved through the capture area and to the waste reservoir. Since this is a washing procedure, this step was repeated until all of the PE buffer was removed from the reservoir. Finally, to release all bound DNA in the capture area, one volume of the EB buffer was pulled and moved through the capture area and deposited in the output reservoir. This elution step was repeated until the full volume of the EB reservoir was transferred to the output reservoir. To confirm completion of each step, the chip was removed from the device in between staged and viewed under a UV microscope. Particular attention was given to the capture area at the post wash – pre elution stage as any unbound DNA should be washed away to waste. Figure 48a shows a remaining concentration of fluorescents after the wash step indicating bound DNA.

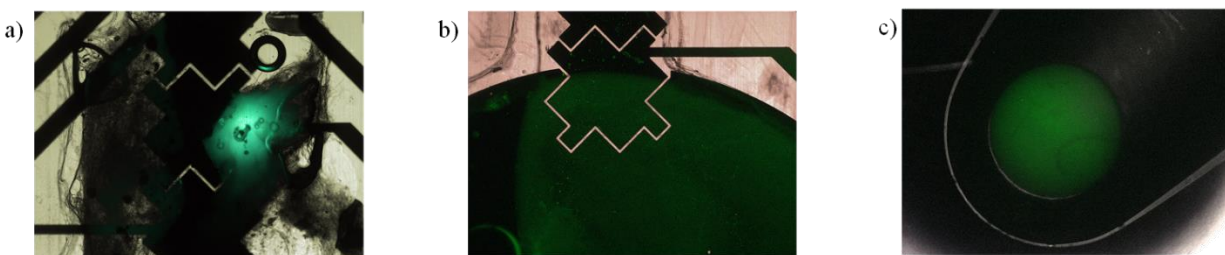


Figure 48 – a) Capture area showing fluorescents after wash. b) Waste reservoir after wash. c) Output of device in Eppendorf tube.

After the elution buffer was moved through the capture area to the output reservoir, the contents of the output reservoir were removed using a pipette and placed into an Eppendorf tube. During the process of removal, silicone oil was extracted along with the DNA concentrated media. Placing the Eppendorf over the UV microscope revealed a small droplet emitting fluorescents suggesting some concentration of DNA was recovered. To evaluate how much DNA was retrieved, only the volume (4 μL) of the DNA concentrated media was removed from the Eppendorf tube, leaving behind the silicone oil. The concentrated DNA solution was placed in a plate well along with 46 μL of a binding buffer. Five, tenfold dilutions of the original fluorescent DNA were made as a reference and placed into five other plate well locations. Additionally, a negative control of just binding buffer was placed in another well. The plate containing all liquids for measure were placed into a plate reader and the results compared. The dilution of the DNA sample used was 10:1 which returned an intensity of 9277608, and the recovered DNA returned an intensity of 331191, suggesting a recovery of 3.6%. While a 3.6% recovery rate may seem small, the results are not discouraging. The

process of manufacturing the capture area is currently a highly variable process causing varying results in the absorption of the lysed sample. It can be seen in Figure 48a that only a small portion of the filter area absorbed DNA material.

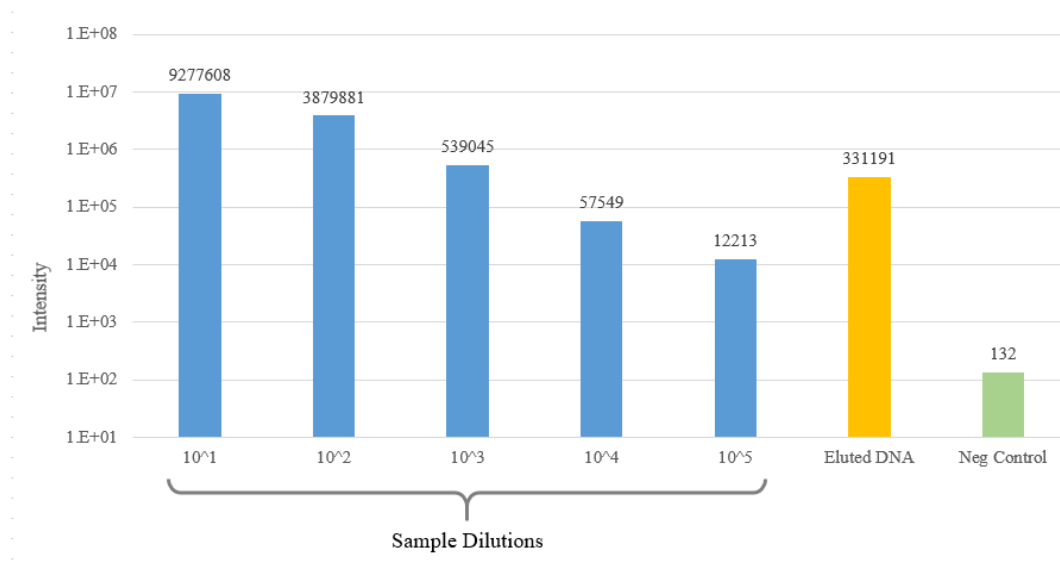


Figure 49 - Plate reader results of DNA Filter protocol

The sample resulting in the rest of the DNA being moved to waste (Figure 48c). Placement of the absorption material is critical for DNA to be absorbed. Even if all material were to absorb the DNA, another issue is that they can become saturated. The size of the capture area is relatively small compared to the volume of sample and PNI that is getting moved through. Therefore, there is more DNA material than the capture area can hold, so the rest gets moved to the waste reservoir. The encouraging part of these results is that it shows the beginnings of a DNA isolation protocol being implemented on a PoC type device. Increasing the recovery rate can be accomplished by increasing the size of the capture area and developing a more consistent manufacturing process of the capture area.

4.5.1.2. MAGNETIC BEAD METHOD

To further demonstrate the ability and diversity of the device, another method for DNA extraction was demonstrated using magnetic beads. The magnetic beads used contain Chitosan which can bind DNA given a slightly acidic pH environment. DNA can then be released from the Chitosan by increasing the pH level of the environment to a less acidic level. To control the pH levels and therefore binding and eluting of DNA, MES buffer (pH 5.0) was used to bind DNA to the beads. Tris buffer (pH 8.8) was used to elute the DNA from the beads. Unlike the filter

method discussed previously, which used a known protocol from a kit, the protocol used for the magnetic beads had to be developed.

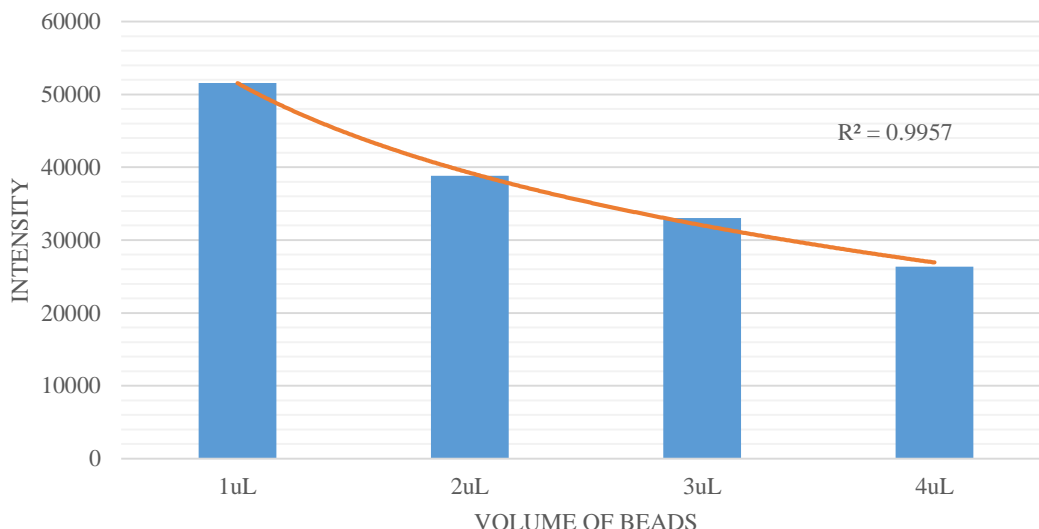


Figure 50 - Unbound DNA for volume of beads

The ratio of magnetic beads to volume of sample was first investigated to understand if there was an optimum or improved binding from one value to another. Figure 50 shows how much DNA was left unbound after mixing 1uL of sample DNA with increasing volumes of magnetic beads. It was found that while increasing the volume of magnetic beads, there are diminishing returns. Since the cost of the Chitosan beads is relatively high, the protocol becomes a tradeoff between cost and performance. It was determined that using a ratio of 3:1 of beads vs DNA was a good compromise. To help ensure that the environment became acidic, a 2:1 volume of MES buffer was mixed with the sample DNA. All three liquids would be mixed together at the appropriate ratios and then transported to a magnetic area to let the DNA bound beads precipitate from the surrounding supernatant. Once separated, the supernatant containing any unbound DNA, is moved and discarded. Tris buffer is then moved through the magnetic area to elute the DNA from the beads, while leaving the beads in magnetic area.

To implement this protocol, the same EWOD chip design as the filter method was used, but the reservoirs were simply filled with different liquids. A different program was written to accommodate the change in activation sequences, and a magnet was incorporated into the device design. Figure 51a shows the locations of the different buffers used as well as the location of the magnet.

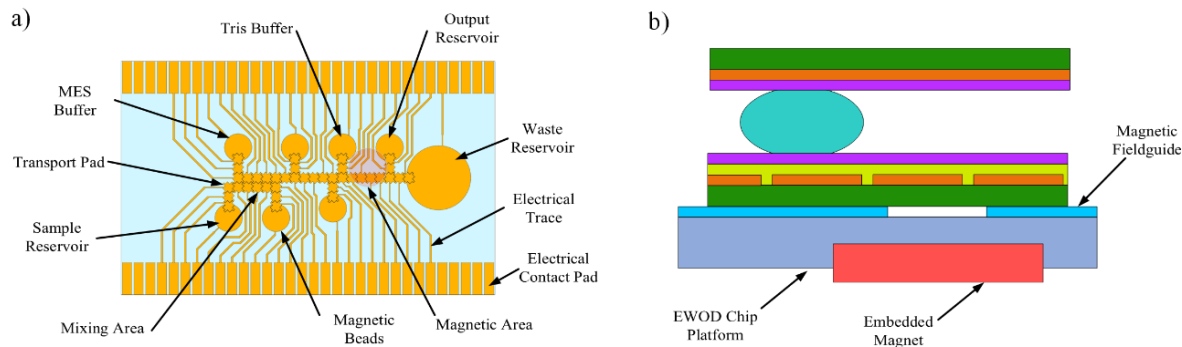


Figure 51 - EWOD device for Magnetic Bead method

The EWOD system could be thought of as a process of controlling the electric field around the droplet. However, with the introduction of a magnet, and magnetic beads, there now exists a magnetic field seen by a large area of the chip. In early tests the magnetic field was strong enough to pull the magnetic solution across of the EWOD chip without initiating or controlling the movement. Experiments were conducted with changing the strength of the magnet, placement, etc., but there is an inherent conflict between unwanted movement and the ability precipitate the beads in solution. A stronger field is better at grouping the magnetic beads and separating them from the solution, however, the magnetic field is only desired in a relatively small area. Reducing the magnetic strength enough to where it no longer affects the droplet outside of the magnetic area, only reduces its effectiveness to precipitate the solution when needed. An answer to this issue was to create a mechanism to guide the magnetic field away from areas it is not desired, while still being strong in where it is needed. Similar to how waveguides focus and shape electromagnetic waves, a “magnetic fieldguide” was created to help shape the magnetic field to better suit this application. Based on the principles of magnetic fields being diverted through a ferromagnetic magnetic material, a metal plate was placed between the EWOD chip and the magnet. To ensure the magnetic field still reaches the beads in the magnetic area, a hole was drilled into the plate to allow the magnetic field to come through. The result is a magnetic field restricted to the area of the hole. Magnetic field that would have stretched across the EWOD chip are now redirected through the metal. Figure 52 - Theoretical magnetic field lines a) without fieldguide and b) with fieldguide shows what the magnetic fields would look like with and without the fieldguide. The magnetic fieldguide was very effective in creating a sharp magnetic field gradient directly above the magnet, and eliminating the effects of the magnet everywhere else allowing to the use of a stronger magnet without the negative effects.

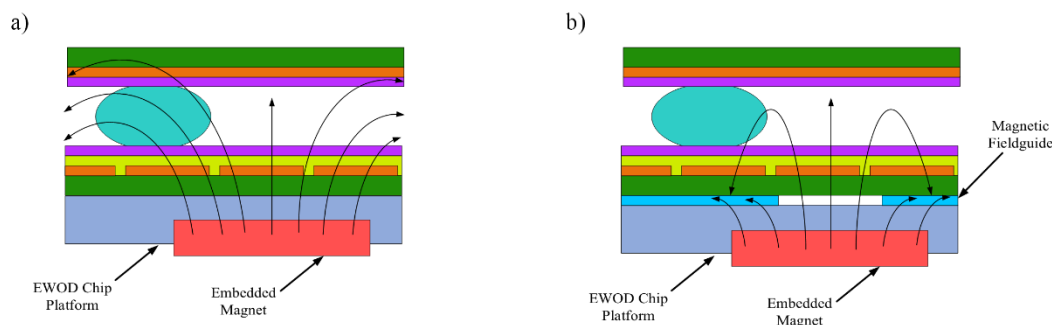


Figure 52 - Theoretical magnetic field lines a) without fieldguide and b) with fieldguide

The magnetic bead protocol was performed as described above where all liquids moved easily in the EWOD device. The mixing step was increased for this protocol to give DNA a better chance to bind to the magnetic beads. The entire volume (~1.5 μ L) of the mixture was moved to the magnet and allowed to settle and precipitate. Once sufficient separation was seen, the majority of the liquid was moved to the waste reservoir leaving the beads over the magnet. Finally, Tris buffer was moved to the magnet area and agitated slightly before to help remove DNA from the beads.



Figure 53 - a) Sample reservoir. b) Waste reservoir with unbound DNA. c) Output reservoir with eluted DNA.

The magnetic beads remained in the magnetic area while the eluted DNA was moved to the output. Fluorescents were checked in the waste reservoir to observe any unbound DNA, which did show a very low level of intensity that was hard to capture in images. The output reservoir, however, showed very high levels of fluorescents which would indicate a high recovery of eluted DNA. The output liquid was removed using a pipette and placed into a plate reader. The output results were compared against 1 μ L of the original sample DNA and MES buffer. Since the protocol used only ~260nL of DNA sample, the results of the sample DNA were divided by for to correct for the difference in volume. Figure 54 shows the plate reader results for the magnetic bead protocol. The intensity of the sample DNA was 77616.25 while the intensity of the output was 72054, suggesting a recovery of 92.8%. The high

recovery rate correlates well with the fluorescent images shown in Figure 53. If the output results were exaggerated from unbound DNA not being sufficiently removed, then that would suggest at least some unbound DNA would have made it into the waste reservoir during removal. Another possible source of contamination would be that magnetic beads bound with DNA made their way to the output reservoir, however, no beads could be observed in the output reservoir.

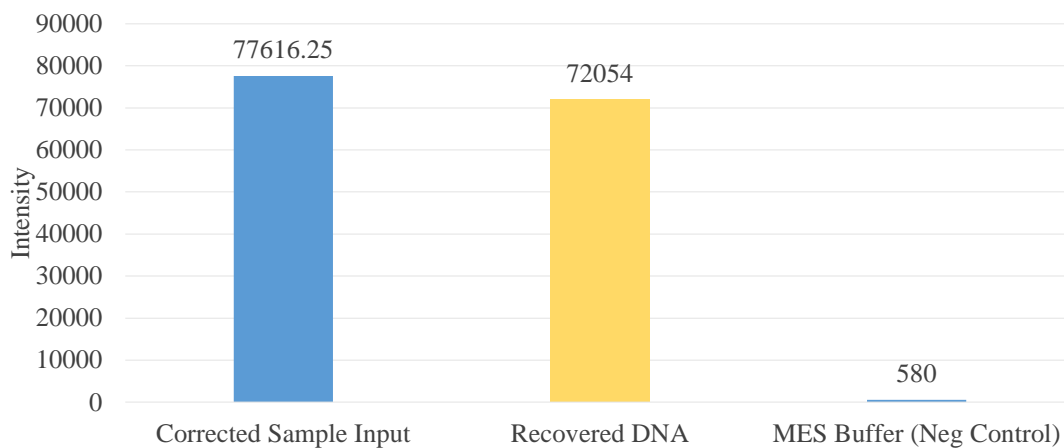


Figure 54 - Plate reader results of Magnetic Beads protocol

Both DNA isolation protocol results are very encouraging for the EWOD system as a whole. The movement of liquids using EWOD has been researched for nearly 20 years [44], yet their use is far from common place. During this research many issues affecting reliability were encountered, suggesting reliability is a limitation to the EWOD design. Issues, such as breakdown, or damage to the surface, which can easily prevent droplet movement. When trying to improve performance by increasing voltage and lowering dielectric thickness, the risk of breakdown increases. Additionally, manufacturing variations make breakdown a very inconsistent phenomenon making the success of an experiment almost a matter of chance. For an EWOD based system to be a practical solution for PoC devices, it must demonstrate reliability. Table 4 shows a comparison of past demonstrations of EWOD droplet movement to this research. The “Moves” column shows the number of droplet movements required to complete the test being performed in the research. A lower number of movements increases the chances of successful test completion due to the lower chance of revealing a weak point in the dielectric layer. However, more complex tests, requiring a high number of movements, will require the EWOD system to be extremely reliable to be successful. It can be seen that the DNA

isolation protocol, using the filter method, requires 500 movements to split, mix, and transport all liquids. A far greater number than other research, and chips were often reused multiple times for different tests.

Research	Test	Practicality (3-6-9)	Moves	Liquid types	FOM
M. Paknahad et al [36]	Droplet Movement	3	2	1	6
J. Gong et al [32]	Droplet Movement	3	20	1	60
N. A. Mousa et al [38]	Tissue Estrogen Assay	9	35	2	630
L. Malica [30]	DNA Hybridization	3	140	3	1260
P.Y. Hung et al [22]	DNA Isolation	6*	50	6	1800
This research	DNA Isolation - Filter	9	500	4	18000

Table 4 - Comparison of this research to past research. *Full protocol not completed

The “Practicality” column uses a 3-6-9 ranking system to assess how useful the test would be in a real world application. For instance, the moving droplets alone does not add much value to research or industry even though they are required to conduct more complex tests. Two research papers that focus on droplet movement were included for comparison reasons. Another measure of how useful the EWOD device can be is the number of liquids moved during the test. Biological samples and reagents have very different properties resulting in very different movement characteristics. Demonstrating movement of many liquids on a single device shows its diversity of capability. To give an overall ranking, and single point of comparison, a Figure of Merit (FOM) was created by multiplying the previous three columns. This research is shown to have the highest FOM mostly from the large number of movements. However, this research deems the number of movements a good indicator of reliability.

Another area this research touches on is other supporting features that help the system translate to a real world device. Much of the past research focuses on only one aspect of the system, such as droplet movement, position feedback, or executing a particular assay [22], [32], [36], [37], [39]. However, there are additional hurdles to overcome if the system were to be implemented in a PoC device. The most common example of this is the process of loading liquids. Many research papers simply pipette the sample and reagents onto the reservoir pads before applying the ground plane. This is acceptable for research applications, but leaves the system impractical for use in industry. Some of these have been examined on an individual basis in prior research, but this research combines many into a single system. Ports were drilled into the glass top plate to allow the loading and removal of all liquids. The chip could also be preloaded with reagents, leaving only the need to add a sample before conducting the assay. Additionally, the system was designed to accept a predefined chip size making it easy to add and remove chips specific to an assay. In

the case of this research, the device was designed around a 1"x3" glass slide with a 128 interfacing contact pads along the side (Figure 32). These contact pads can then be connected to transport pads or reservoirs in patterns to suit any number of assays. The on board memory is large enough to store multiple test programs, so switching between tests is simply a matter of swapping chips and selecting the appropriate program. Another way this research tries to move closer to a complete solution is by incorporating all of these features onto a small, battery powered, device. Even if other research addresses loading and control methods, most activation signals are produced using bench top signal generators and amplifiers. Feedback signals are often processed using a PC or laptop. This research may be the first to demonstrate a system which can operate in the field without supporting equipment.

CHAPTER 5 – CONCLUSIONS AND FUTURE WORK

A digital microfluidic device using EWOD in a small hand-held platform capable of performing many sample preparation tasks automatically has been presented in this thesis. A set of design principles for PoC applications were discussed, and more importantly, the challenges of different design aspects and their potential solutions were presented in detail. An industry standard sample prep protocol for extraction and isolation of DNA has been demonstrated to illustrate the stated capabilities of the proposed device. The device requires a fraction of the liquids lab-based methods use, which greatly reduces the cost per test. Table 5 compares the amount of liquid used by the proposed device with the amount of liquid used per Nucleotide Removal Kit by Qiagen for the same task. It is seen that due the small size of the EWOD system, and small fraction of reagents are required to conduct the protocol, which can greatly lower testing costs. Since the resolution of the volumes moved by the EWOD device are determined by the pad geometry and ground height, given the same pad geometry, the volumes spit from the reservoirs will be the same. Therefore, the volumes can be considered in terms of “units”, where one unit is the volume to cover one pad. For reference, the last column in Table 5 lists the number of volumes pulled from the reservoirs to accommodate the ratios specified by the protocol.

Standard DNA Protocol	Vol (uL)		
Add Sample	150		
Add PNI Buffer	750		
Transfer mixture to column.			
Centrifuge			
Add PE Buffer	750		
Centrifuge			
Add Elution Buffer	150		
Centrifuge			
Purified DNA			
Total volume (uL)	1800		

Device DNA Protocol	Vol (uL)	Unit Vols
Pull Sample	0.26	1
Pull PNI Buffer	1.3	5
Move mixture to filter		
Pull PE Buffer	1.3	5
Move buffer through filter to waste		
Pull Elution Buffer	0.78	3
Move Elution Buffer through filter to output		
Purified DNA		
Total volume (uL)	3.64	
% less volume	494.51	

Table 5 - Protocol and volume comparison of Qiagen kit and this research

The results shown in this thesis demonstrate a promising step forward for more practical applications of EWOD in sample prep. Future work to further expand the capabilities of the proposed platform includes:

5.1. SENSOR INTEGRATION

The logical addition to a device that can automate sample preparation on such a small scale would be a sensor to make use of the prepared sample. Indeed, much research has been done on sensor technology that can detect pathogens in various ways. Affinity sensors offer impressive specificity and limits of detection in a small foot print, and would incorporate easily into the EWOD sample prep chip. The combination of sample prep and sensing offers the possibility for a complete Point of Care device, which has yet to be seen in the industry or research. Briefly, affinity sensors contain a biological material that is immobilized onto the sensor (probe), which is known to attract a specific analyte (target). Multiple sensors could be arranged on the EWOD chip where each sensor could sense a different analyte, which would allow the device to screen for multiple diseases with one prepared sample. Being able to search for several diseases at once would be beneficial for situations where symptoms are similar between many diseases. For instance, West Nile and Ebola have similar symptoms as Influenza in their early stages. Another promising application could be screening for diseases or bacteria common for a particular environment. Doctors and nurses have to monitor and treat infections which are common to hospitals and clinics, such as Methicillin-Resistant Staphylococcus Aureus (MRSA) and Clostridium Difficile (C-Diff). When found, appropriate treatment or quarantine procedures must be executed to prevent the spread of infection to other patients or the care givers themselves. An EWOD chip embedded with sensors able to detect common infections of patients could quickly and easily alert care givers of infected patients and take appropriate actions to reduce the chance of spreading. Multiple sensors could also provide the opportunity to take multiple measurements of the same analyte to increase reliability of the results by taking the average or by applying other statistical methods. The electronics needed to support such sensors is also relatively minimal and could be incorporated into the microcontroller used to control the sample prep. Therefore, sensor functionality could be added with virtually no increase in device size.

5.2. RNA ISOLATION

While this research demonstrated DNA isolation, RNA isolation would be another protocol to investigate. Much of the procedures are the same between isolating DNA and RNA, however, RNA degrades much easier than DNA and requires more attention to sterilization, particularly from Ribonuclease (RNase). To help ensure RNA quality of the output results, analysis using gel electrophoresis would need be done to determine if the RNA was degraded during the process. In the early stages it was unknown if the EWOD device would contribute to RNA degradation or if RNase contamination would be the only reason. Establishing DNA isolation as a baseline now offers the opportunity

to investigate RNA isolation while focusing on RNase contamination. The EWOD design being used in this research may offer the ability to reduce the risk of contamination due to the oil media in which it operates. The device would be cleaned ahead of time, but the oil media may help ensure the sample and reagents remain free of the surfaces and potential contamination. Essentially, the oil may act as a protective barrier as it moves liquids.

5.3. PCB EWOD CHIP DESIGN

As seen in Figure 10, the use of other materials for the EWOD system have been investigated with varying results. Much of the testing was done using Printed Circuit Board (PCB) based chips, where the pad array was created using typical PCB manufacturing techniques. As mentioned previously, the relatively thick layers of copper used in PCBs caused unwanted droplet splitting. There were also questions early in this research if the PCB technique could be used due to the larger feature sizes inherent to the PCB process compared to photolithography. The minimum feature size for the typical PCB manufacturing processes is roughly 200 μm , where photolithography is near 20 μm . Research done in this thesis on pad design may minimize the negative effects from large distances between pads. Additionally, adding a dielectric material to reduce the effective thickness of the copper is also a possibility worth investigating, since it was found in this research that the point of failure is seldom between pads, but rather between the active pad and the droplet through a weakness in the dielectric layer. The dielectric strength between pads comes from the relatively large distance between pads, which is inherent in the PCB process. Therefore, a material with a lower dielectric strength can be used to fill the gap between pads, which greatly increases material options. However, coating the top layer with a high dielectric strength material such as Parylene – C would still be required.

5.4. SYSTEM DESIGN IMPROVEMENTS

While the design presented in this research is effective and offers a solid foundation to build on, improvements were noticed that could make the device more practical. One of the areas where this thesis had a hard time reaching its goals was in generating the highest voltage levels of the high voltage output. A more complex SMPS design may be able to obtain higher voltage levels while, at the same time, become more responsive to system loads. A synchronous multiphase boost converter incorporates multiple boost converters in parallel. Synchronizing the switching of each converter in such a way that they are out of phase with each other reduces current ripple seen at the output. Additionally, they can be enabled according to system load, which is ideal for the dynamic demands of the

activation voltage. Inductor sizes of each boost converter can also be reduced which increases the di/dt of the power supply.

Reducing complexity of the circuit could be done by selecting a more capable microcontroller to handle both the main device interactions as well as the USB communication. Development of this work was intentionally built based on current Arduino designs. Being able to leverage Arduino's supporting systems such as IDE, schematics, open source libraries, etc. made it possible to quickly develop prototypes and establish a known working state. However, there now exists a working state and supporting code that is several steps removed from an Arduino, which enables the freedom to be more creative with component selection.

REFERENCES

- [1] M. P. McRae *et al.*, “Programmable bio-nano-chip system: a flexible point-of-care platform for bioscience and clinical measurements,” *Lab Chip*, vol. 15, no. 20, pp. 4020–4031, 2015.
- [2] M. Zarei, “Biosensors and Bioelectronics Infectious pathogens meet point-of-care diagnostics,” *Biosens. Bioelectron.*, vol. 106, no. January, pp. 193–203, 2018.
- [3] Y. Hou, J. Wang, Y. Jiang, C. Lv, L. Xia, and S. Hong, “Biosensors and Bioelectronics A colorimetric and electrochemical immunosensor for point-of-care detection of enterovirus 71,” *Biosens. Bioelectron.*, vol. 99, no. July 2017, pp. 186–192, 2018.
- [4] “Abbott Point of Care | i-STAT System & Piccolo Xpress.” [Online]. Available: <https://www.pointofcare.abbott/us/en/home>. [Accessed: 08-Jun-2018].
- [5] W. A. Schell *et al.*, “Evaluation of a digital microfluidic real-time PCR platform to detect DNA of *Candida albicans* in blood,” *Eur. J. Clin. Microbiol. Infect. Dis.*, vol. 31, no. 9, pp. 2237–2245, 2012.
- [6] D. Stirling and M. S. J. Bartlett, *PCR Protocols Second Edition*. 2003.
- [7] J. M. S. Bartlett and D. Stirling, “A Short History of the Polymerase Chain Reaction,” in *PCR Protocols*, 2003.
- [8] B. C. Delidow, J. P. Lynch, J. J. Peluso, and B. a White, “Polymerase Chain Reaction,” *PCR Protoc.*, 1993.
- [9] J. Lu, S. Ge, L. Ge, M. Yan, and J. Yu, “Electrochemical DNA sensor based on three-dimensional folding paper device for specific and sensitive point-of-care testing,” *Electrochim. Acta*, vol. 80, pp. 334–341, 2012.
- [10] K. Ren, J. Wu, F. Yan, Y. Zhang, and H. Ju, “Immunoreaction-triggered DNA assembly for one-step sensitive ratiometric electrochemical biosensing of protein biomarker,” *Biosens. Bioelectron.*, vol. 66, pp. 345–349, 2015.
- [11] L. Wang, M. Veselinovic, L. Yang, B. J. Geiss, D. S. Dandy, and T. Chen, “A sensitive DNA capacitive biosensor using interdigitated electrodes,” *Biosens. Bioelectron.*, 2017.
- [12] T. Scientific, “QuickClean II PCR Extraction Kit Technical Manual No . 0595 Cat . No . L00419 Version : 08272013,” vol. 100, no. 0595. pp. 1–5.
- [13] Q. Gel and E. Kit, “Quick-Start Protocol October 2010 Sample & Assay Technologies Quick-Start Protocol Sample & Assay Technologies,” no. March 2008, pp. 12–13, 2010.

- [14] T. Wizard and L. Solution, “Wizard ® Genomic DNA Purification Kit,” no. 050, pp. 1–16.
- [15] “QIAquick Nucleotide Removal Kit - QIAGEN.” [Online]. Available: <https://www.qiagen.com/us/search/qiaquick-nucleotide-removal-kit/>. [Accessed: 09-Jun-2018].
- [16] T. Baier *et al.*, “Hands-free sample preparation platform for nucleic acid analysis,” *Lab Chip*, vol. 9, no. 23, p. 3399, 2009.
- [17] C. Rivet, H. Lee, A. Hirsch, S. Hamilton, and H. Lu, “Microfluidics for medical diagnostics and biosensors,” *Chem. Eng. Sci.*, vol. 66, no. 7, pp. 1490–1507, 2011.
- [18] D. C. Leslie *et al.*, “Frequency-specific flow control in microfluidic circuits with passive elastomeric features,” *Nat. Phys.*, vol. 5, no. 3, pp. 231–235, 2009.
- [19] C. Phurimsak *et al.*, “Phaseguide assisted liquid lamination for magnetic particle-based assays,” *Lab Chip*, vol. 14, no. 13, pp. 2334–2343, 2014.
- [20] F. R. De Souza, G. L. Alves, and W. K. T. Coltro, “Capillary-driven toner-based microfluidic devices for clinical diagnostics with colorimetric detection,” *Anal. Chem.*, vol. 84, no. 21, pp. 9002–9007, 2012.
- [21] T. S. Park and J.-Y. Yoon, “Smartphone Detection of *Escherichia coli* From Field Water Samples on Paper Microfluidics,” *IEEE Sens. J.*, vol. 15, no. 3, pp. 1902–1907, 2015.
- [22] P.-Y. Hung, P.-S. Jiang, E.-F. Lee, S.-K. Fan, and Y.-W. Lu, “Genomic DNA extraction from whole blood using a digital microfluidic (DMF) platform with magnetic beads,” *Microsyst. Technol.*, 2015.
- [23] S. H. Au, P. Kumar, and A. R. Wheeler, “A new angle on Pluronic additives: Advancing droplets and understanding in digital microfluidics,” *Langmuir*, vol. 27, no. 13, pp. 8586–8594, 2011.
- [24] R. B. Fair, *Digital microfluidics: Is a true lab-on-a-chip possible?*, vol. 3, no. 3. 2007.
- [25] P. M. Young and K. Mohseni, “Force characterization of dielectrophoresis in droplet transport,” *Ann. N. Y. Acad. Sci.*, vol. 1161, pp. 463–471, 2009.
- [26] D. Bakewell, N. Vergara-Irigaray, and D. Holmes, “Dielectrophoresis of Biomolecules,” *JSM Nanotechnol. Nanomedicine*, vol. 1, no. 1003, pp. 1–14, 2013.
- [27] K. Choi, A. H. C. Ng, R. Fobel, and A. R. Wheeler, “Digital Microfluidics,” *Annu. Rev. Anal. Chem.*, vol. 5, no. 1, pp. 413–440, 2012.
- [28] K. Choi, A. H. C. Ng, R. Fobel, and A. R. Wheeler, “Digital microfluidics,” *Annu. Rev. Anal. Chem. (Palo Alto, Calif.)*, vol. 5, pp. 413–40, 2012.
- [29] L. Li, H. Hu, H. Lin, and D.-T. Ye, “Electrowetting of the blood droplet on the hydrophobic film of the EWOD

- chips.,” *Conf. Proc. ... Annu. Int. Conf. IEEE Eng. Med. Biol. Soc. IEEE Eng. Med. Biol. Soc. Annu. Conf.*, vol. 2, pp. 1941–4, 2005.
- [30] L. Malic, T. Veres, and M. Tabrizian, “Biochip functionalization using electrowetting-on-dielectric digital microfluidics for surface plasmon resonance imaging detection of DNA hybridization,” *Biosens. Bioelectron.*, vol. 24, no. 7, pp. 2218–2224, 2009.
- [31] V. Srinivasan, V. K. Pamula, and R. B. Fair, “An integrated digital microfluidic lab-on-a-chip for clinical diagnostics on human physiological fluids.,” *Lab Chip*, vol. 4, no. 4, pp. 310–315, 2004.
- [32] J. Gong and C. Kim, “Direct-Referencing Two-Dimensional-Array Digital Microfluidics Using Multilayer Printed Circuit Board,” *Access*, vol. 17, no. 2, pp. 257–264, 2008.
- [33] Y. Li, R. Chen, and R. J. Baker, “A fast fabricating electro-wetting platform to implement large droplet manipulation,” *Midwest Symp. Circuits Syst.*, pp. 326–329, 2014.
- [34] C. H. Chen, S. L. Tsai, M. K. Chen, and L. S. Jang, “Effects of gap height, applied frequency, and fluid conductivity on minimum actuation voltage of electrowetting-on-dielectric and liquid dielectrophoresis,” *Sensors Actuators, B Chem.*, vol. 159, no. 1, pp. 321–327, 2011.
- [35] H. Ren, R. B. Fair, and M. G. Pollack, “Automated on-chip droplet dispensing with volume control by electrowetting actuation and capacitance metering,” *Sensors Actuators, B Chem.*, vol. 98, no. 2–3, pp. 319–327, 2004.
- [36] M. Paknahad, H. R. Nejad, and M. Hoorfar, “Development of a digital micropump with controlled flow rate for microfluidic platforms,” *Sensors and Transducers*, vol. 183, no. 12, pp. 84–89, 2014.
- [37] T. Lederer, S. Clara, B. Jakoby, and W. Hilber, “Integration of impedance spectroscopy sensors in a digital microfluidic platform,” *Microsyst. Technol.*, vol. 18, no. 7–8, pp. 1163–1180, 2012.
- [38] N. A. Mousa *et al.*, “Droplet-scale estrogen assays in breast tissue, blood, and serum.,” *Sci. Transl. Med.*, vol. 1, no. 1, p. 1ra2, 2009.
- [39] S. C. C. Shih, I. Barbulovic-Nad, X. Yang, R. Fobel, and A. R. Wheeler, “Digital microfluidics with impedance sensing for integrated cell culture and analysis,” *Biosens. Bioelectron.*, vol. 42, no. 1, pp. 314–320, 2013.
- [40] N. Kumari, V. Bahadur, and S. V. Garimella, “Electrical actuation of electrically conducting and insulating droplets using ac and dc voltages,” *J. Micromechanics Microengineering*, vol. 18, no. 10, 2008.

- [41] B. Brazey, J. Cottet, A. Bolopion, H. Van Lintel, P. Renaud, and M. Gauthier, “Impedance-based real-time position sensor for lab-on-a-chip devices,” *Lab Chip*, 2018.
- [42] M. A. Murran and H. Najjaran, “Capacitance-based droplet position estimator for digital microfluidic devices,” *Lab Chip*, vol. 12, no. 11, p. 2053, 2012.
- [43] S. C. C. Shih, R. Fobel, P. Kumar, and A. R. Wheeler, “A feedback control system for high-fidelity digital microfluidics,” *Lab Chip*, vol. 11, no. 3, pp. 535–540, 2011.
- [44] M. G. Pollack, R. B. Fair, and A. D. Shenderov, “Electrowetting-based actuation of liquid droplets for microfluidic applications,” *Appl. Phys. Lett.*, vol. 77, no. 11, p. 1725, 2000.

APPENDIX A – MEMORY DATA FORMAT

Address	Size	Memory Word (1 byte)										
		7	6	5	4	3	2	1	0			
0x000	2 Bytes	Number of programs loaded								System Info		
		:										
	2 Bytes	Starting Address of Program 1										
		:										
	2 Bytes	Starting Address of Program 2										
		:										
		:										
	2 Bytes	Starting Address of Program N - L										
		Starting Address of Program N - L										
	10 Bytes	Program 1 Name								Header Info		
		:										
		:										
	1 Byte	Activation Voltage								Header Info		
	2 Bytes	Number of Sequences										
		:										
	16 Bytes	Sequence 1								Protocol Info	Program 1	
		:										
		:										
	2 Bytes	Threshold Level 1										
		:										
		:										
	16 Bytes	Sequence 2										
		:										
		:										
	2 Bytes	Threshold Level 2										
		:										
		:										
	N Bytes	:										
	:	:										
	:	:										
		Sequence N										
		:										
		:										
	2 Bytes	Threshold Level N										
		:										
		:										
		Program 1 Name								Header Info		
		:										
		:										
		Activation Voltage								Header Info		
		Number of Sequences										
		:										
		Sequence 1								Protocol Info	Program 2	
		Sequence 2										
		:										
		:										

APPENDIX B – DEVICE FIRMWARE WORKFLOW

